AD NUMBER

AD488153

NEW LIMITATION CHANGE

TO

Approved for public release, distribution unlimited

FROM

Distribution authorized to U.S. Gov't. agencies and their contractors; Administrative/Operational Use; MAR 1966. Other requests shall be referred to Air Force Materials Laboratory, Attn: Research & Technology Division, Wright-Patterson AFB, OH 45433.

AUTHORITY

AFML ltr, 7 Dec 1972

AFML-TR-66-40

HYPERVELOCITY IMPACT STUDIES

Robert F. Rolsten
Technical Operations Research

TECHNICAL REPORT NO. AFML-TR-66-40
March 1966

Air Force Materials Laboratory
Research and Technology Division
Air Force Systems Command
Wright-Patterson Air Force Base, Ohio

HYPERVELOCITY IMPACT STUDIES

Robert F. Rolsten

Technical Operations Research

FOREWORD

This final report (TO-B 65-103) contains the results of a nine-month study (1 February to 15 October 1965) conducted by Technical Operations Research in compliance with Air Force Contract AF 33(615)-01333. The report was submitted in draft form by the author on 15 October 1965.

This program was conducted under the direction of Mr. A.K. Hopkins (MAYH) of the AF Materials Laboratory, Research and Technology Division, Wright-Patterson Air Force Base.

The author wishes to express his appreciation to the many individuals who provided valuable support and assistance during this program. The following deserve particular recognition:

Messrs. C.H. Bagley and T.E. Holland for their excellent critique of experimental concepts.

Dr. E.F. Poncelet and Mr. H.H. Hunt for their development and critique of theoretical concepts.

Mr. R.W. O'Neil for selected exploding-foil gun experiments.

Mr. John Nunes of the U.S. Army Material Research Agency for the establishment of the mechanical property data for the aluminum targets.

Utah Research and Development Corporation for selected high-velocity impact experiments.

Lts. A.J. Holten and W.A. Dean of the United States Air Force for providing impact testing and metallurgical evaluation assistance.

The manuscript was released by the author on 15 October 1965 for publication as an RTD technical report.

This technical report has been reviewed and is approved.

RICHARD J. VOSSLER, Chief
High Energy Physics Branch
Materials Physics Division
AF Materials Laboratory

ABSTRACT

Two different problems related to hypervelocity impact were studied. The first involved the formation of a rippled surface produced at the interface of a stack of plates impacted by a projectile. The rippled structure was produced, as observed in cross section, as a sine wave, a sawtooth structure, and as oriented waves with a peaked crest. Some plates were welded permanently; others separated as a result of failure in the base metal. A plausible explanation for the ring structure was found. The second problem involved the preparation and evaluation of homogeneous 1100-0, 7075-0, and 7075-T6 aluminum ingots for use as hypervelocity impact targets. An attempt was made to control grain size and to provide equiaxed grains. Tensile test data obtained in longitudinal and transverse specimens include yield and ultimate and true stress to fracture.

TABLE OF CONTENTS

TABLE OF CONTENTS (Cont'd.)

LIST OF ILLUSTRATIONS

LIST OF ILLUSTRATIONS (Cont'd.)

LIST OF TABLES

INTRODUCTION

This program was concerned primarily with the response of materials to hypervelocity impact. In the design of space equipment, consideration must be given to the effects of possible impacts by natural or artificial particles traveling at velocities far in excess of those possible in the earth environment. The chances of puncture with a resulting loss of essential fluids, detonation of tankage or rupture of tanks by strong shock waves, damage by high velocity spall fragments, and introduction of interruptions in the aerodynamic flow patterns of reentry vehicles or supersonic aircraft are types of impact damage that are of grave concern.

An important part of this program involved cataloguing and evaluating phenomena that acquire importance and notice as a consequence of ventures into realms of higher and higher velocities for both vehicles and material environments.

Impact theory and structural design have generally followed separate paths, and few attempts have been made to integrate theoretical concepts and recognized phenomena in the development of structural systems. The prime prerequisite for the establishment of realistic design criteria is a systematic experimental and theoretical investigation carried out on materials and structural configurations useful in actual vehicle design. Such a systematic approach should also permit an expeditious revision of design criteria when new environmental or other parametric data become available.

In the progress reports covering the first phase of this contract, primary emphasis was placed on the welding of metal plates by hypervelocity impact and on phenomena of rippled surfaces produced with and without welding. These reports were prepared to record and reflect the progress of the work during each phase of the program development. Conclusions drawn and concepts developed were tentative only and based on data available at the time of reporting.

Part I of the report refines all the experimental and theoretical data collected during the program and develops the tentative concepts into a synthesis of individual relationships in order to evolve the principles of ripple formation of a surface impulsively loaded by impact with a hypervelocity particle.

Part II of the report describes the procedures that were necessary to procure a quantity of homogeneous alloy aluminum suitable for hypervelocity impact testing experiments. Homogeneity was established by examination of the microstructure and by tensile testing of specimens prepared from both the transverse and longitudinal portions of the ingot and at temperatures ranging from +24 to - 196°C.

PART I

EFFECTS OF OBLIQUE SHOCKS PRODUCED AT METAL INTERFACES P HYPERVELOCITY PARTICLE IMPACT

During this contract, the effects of hypervelocity microparticle impacts on a stack of aluminum targets were investigated experimentally. We observed that spot welding and rippling can be brought about by the action of the high velocity projectile on the materials comprising the projectile-target interface. To arrive at an explanation for the formation of the rippled structure with or without welding, it is necessary to discuss the role of particle impact on a stack of plates and the shock disturbances in the top plate as well as the subjacent plate.

A strong shock wave sweeping along the interface of two metal plates held in contact may leave a pattern of ripples on both surfaces of the mating faces. These ripples have been observed to form under a variety of impact loading conditions, ranging from the impact of bullets at oblique angles on plates, the collisions of two plates accelerated with explosives, and in the impulsive load area of a stack of plates impacted with a hypervelocity particle.

Allen et al.[1] reported rippled surface deformations on 0.50-caliber right-circular steel cylinders after these had been fired into thin lead targets at oblique angles. The surface structure consisted of a region of more-or-less parallel ripples across the nose of the projectile. A near circular ring of a galled or fretted surface has been observed surrounding the impact craters or holes on the mating surfaces of target plates that had been in intimate contact during hypervelocity impact.[2] Part of the surface within these galled rings was marked with a series of concentric ripples.

Pearson[3,4] observed a ripple structure at the explosively welded interface of metal plates when the welding was accomplished by driving the plates together at an oblique angle. In our experiments, when stacks of aluminum and of aluminum and copper plates were impacted by a microparticle at hypervelocity, spot welding was observed in association with interlocking rippled interfaces. Abrahamson[5] also noted that rippled surfaces were formed on the tapered surfaces of projectiles that impacted thin plates and on the interfaces when thin metal plates were driven onto thicker plates at oblique angles by high explosives. Abrahamson also experimented with soft materials, such as grease and silicone putty, and was successful in reproducing a wave on these surfaces by impingement with high velocity jets of air and of water.

As we have already pointed out, the formation of these ripples has been generally attributed to "surface jetting." Allen et al.[1] suggested the existence of a critical angle between the planes of the impacting surfaces below which the surface rippling would not occur. This critical angle was theoretically treated by Walsh et al.[6] and by Cowen and Holtzmann.[7] However, Bayce and Wright[8] concluded that the angle was critical only in the sense that it influences the sweep velocity of the collision point over the metals. Both the galled rings and the structure of concentric ripples overlying the ring of disturbed material have been attributed to a difference in relative motion of the mating faces of the plates and to plastic deformation.[2]

PHENOMENA

PARTICLE IMPACT

Particle impact at hypervelocities (velocities in excess of the sonic velocity of the material) are inelastic, since the materials strength is exceeded. The process of momentum transfer is accompanied by destructive work on the projectile and target materials. In this type of impulsive loading (a high load both applied and removed in a very short period of time), acceleration is the dominant factor. Stresses are transient and highly localized. Deformations and fractures may occur in one part of a system quite independent of what happens in another part, which is typical behavior for an impulsively loaded system.

Material at the point of impact is compressed to pressures considerably in excess of the compressive strength of the materials involved. The constraints on the materials in the affected region are not limited by material strength but by the inertial forces, and equations based on elasticity or rigidity for estimating material behavior are invalid in this initial phase of impact. Since significant parameters associated with solids and fluids are identical during this phase, mathematical solutions based on hydrodynamic theory are appropriate for describing behavior in the initial phase. Thus, target and projectile materials flow both forward and laterally into the target. Experimental projectiles are usually short cylinders (discs) or spheres. The factors of greatest concern to us are those involved in a shock reflection.

A high velocity impulsive impact is transmitted through a medium in the form of a shock pulse, or shock wave. The disturbance takes the form of a wave propagating radially outward from the point of impact. High pressure and flow in the region of the inelastic wave produce heating that increases the velocity of its propagation and causes the lagging parts of the surge to catch up with leading parts. Thus a well-defined shock wave with an abrupt front emerges a short distance from the point of impact. If a stationary material of normal density, temperature, and pressure is overrun by a shock front, it is immediately changed to a state of much higher density, temperature, and pressure.

As the wave expands radially outward, any initial eccentricity becomes less pronounced and the wave front approaches a hemispherical configuration. As it expands, it distributes its energy over an increasingly large area. There is an irreversible absorption of mechanical energy by the target material through which the wave is passing. These processes result in a decay of pressure and, in turn, a progressive decay of the hydrodynamic wave until elastic-wave characteristics become dominant. The cavity produced in the target material expands at a velocity of the shocked material which is much lower than that of the shock wave. When a stack of metal plates is impacted, the target material's velocity across such an interface separates the plates with considerable violence.

WAVE PROPAGATION

Propagation of the disturbance in a stack of plates is described by wave phenomena: elastic wave, plastic or hydrodynamic wave, shock wave, reflection of waves at free or rigid boundaries, transmission of waves across interfaces, and attenuation of waves.

1. Elastic Wave

If ρ_o and v_o are the specific gravity and the original velocity of the missile, and ρ the specific gravity of the plate, conservation of momentum requires the mass velocity v in the disturbance created in the plate to be

$$v = \frac{\rho_o}{\rho_o + \rho} v_o \quad .$$

If c is the velocity with which the disturbance is propagated into the plate, conservation of mass requires that the radial compressive deformation ϵ_r of the plate in the radial direction be

$$\epsilon_r = \frac{c - v}{v} \quad .$$

If E and ν are Young's modulus and Poisson's ratio for the plate material, the theory of elasticity requires that the radial or frontal pressure of the disturbance producing such a compression be

$$\sigma_r = \frac{(1 - \nu) E \epsilon_r}{(1 + \nu)(1 - 2\nu)} \quad ,$$

and the lateral or side pressure normal to the front be

$$\sigma_s = \frac{\nu E \epsilon_r}{(1 + \nu)(1 - 2\nu)} = \frac{E \epsilon_r}{(1 + \nu)(1 - 2\nu)} - \sigma_r$$

2. Plastic or Hydrodynamic Wave

If the shear stress $(\sigma_r - \sigma_s)$ greatly exceeds the limit of elasticity, which it presumably does, the metal "flows" within the front of the disturbance, the lateral or side pressure rapidly increases to reach the magnitude of the radial pressure, the compression increases, and the propagation velocity of the disturbance decreases. The propagation of the disturbance has become a hydrodynamic wave and the theory of elasticity ceases to apply. A new relation between the pressure and volume or density that is no longer linear takes over by using a theory closely associated with hydrodynamics. The heating process that takes place within the front of the wave necessitates deviating from the classic theory of hydrodynamics.

3. Shock Wave

The heating process produced by the flowing of the metal raises the temperature of the medium quite significantly and, according to the hydrodynamic theory, causes a corresponding increased propagation rate. Thus it is found that the crest of the wave begins to catch up with the leading foot of the wave and, when close enough, heats the material through which the foot of the wave is passing, which causes every part of the following wave to proceed considerably faster than the usual theory of hydrodynamics would indicate. To permit a sufficiency of heat transfer to induce all parts of the wave to propagate at the same velocity, the whole wave front must be very thin or

"steep," since the amount of heat transfer obeys "Ohm's law" and thus is inversely proportional to the thickness of the layers through which it must pass. The propagation of the disturbance thus described is a shock wave and obeys the theory of Hugoniot shocks.

The preceding phenomena arise so rapidly that it is customary to assume that the shock wave is generated at the instant of impact. Transitory phenomena are usually ignored. They do exist, however, as evidenced for instance by the fact that when the Hugoniot wave propagation rate is less than that of the elastic waves, an elastic wave will run ahead of the shock wave.

4. Reflection of Waves

a. At Free Boundaries. When a wave encounters a free boundary, the pressure and the associated compression disappear suddenly. The resulting expansion practically doubles the material velocity, since it is the original mass velocity that induced the pressure to rise in the first place. This sudden disturbance in the wave front propagates backwards as a "relief" wave, behind which the pressure is nil and the mass velocity about double its previous value. No tensile stresses are generated so far, because we are not considering periodic waves. These considerations hold true for elastic, plastic, and shock waves that meet a free boundary head-on.

b. At Rigid Boundary. When a wave encounters a rigid boundary, the condition is reversed in the sense that the particle velocity is suddenly stopped, thus inducing the same phenomenon as an impact. In the case of elastic waves, where the pressures induced are moderate, such a rigid boundary causes simply a doubling of the pressure and a stopping of the material velocity. The disturbance propagates back from the boundary as rigid reflection. For oblique reflections, only the normal component of the mass velocity is stopped. In particular, the collision of two elastic waves in fact constitutes a true collision at a rigid boundary. Because of the linearity of the stress-strain curve and the constancy of propagation of the disturbance, the collision appears as if each wave had penetrated the other one unhindered.

In the case of plastic and shock waves, the pressures generally exceed the range in which the pressure-compression curve is linear, and the propagation rates are no longer constant; thus collision pressures are apt to exceed the sum of incident and reflecting waves. In oblique reflections, this may lead to situations in which the "reflected" wave is faster than the incident wave and reinforces the incident wave forming a "Mach stem."

When a longitudinal wave strikes a boundary between two similar materials, theoretically no part of it is reflected, since the total wave is transmitted. If the materials are dissimilar, part of the stress wave will be transmitted or refracted and part will be reflected. In the experiments considered, the plates are held together firmly by bolting or clamping.

In theory, if the plates are of similar materials, the shock wave should travel through the entire stack of plates to the last surface of the last plate before being reflected as a relief wave. Actually there is probably some degree of reflection at each interface, since the boundaries are not in absolute contact at every point. The interface does, in fact, move under the impact pressure, producing deformations in the interfaces ahead of the advancing cavity.

5. Attenuation of Waves

In first approximation, elastic waves do not attenuate. They keep on reflecting from boundary to boundary producing sound waves in the air and prolonged ringing. Eventually all their energy has dissipated by such phenomena not taken into account in the simple theory. Their intensity, however, attenuates in spherical waves and rebuilds by interactions.

Plastic and shock waves, however, attenuate sharply because they are energy-absorbing phenomena, transforming the mechanical work spent in flow into thermal energy. The relation between the amount of energy absorbed, the amount of deformation obtained, and final temperature of a specimen through which such waves have propagated is most complex for several reasons. First, the amount of energy absorbed by flow is a function of the rate of flow. Very slow deformations require less energy than very fast ones. Second, the amount of energy dissipated results in increased temperature of the medium which, in effect, works against the dissipation of further energy, because less work is required to perform a given amount of deformation if the temperature is higher. Thus, depending on the rate of deformation, a stable temperature is eventually reached at which a given amount of deformation is achieved at the expense of a given amount of energy, and this given amount of deformation progresses along the specimen.

In the formation of the hypervelocity crater in aluminum, it may be shown by microhardness examination of the plates that the movement of material significantly increased the temperature. The following hardness profile has been repeatedly observed: low hardness adjacent to the crater due to the thermal stress relief; rapidly increasing hardness with increasing distance from the crater until a maximum hardness is observed; and rapidly decreasing hardness from the maximum value to the base hardness of the region unaffected by shocks.

Unless constantly supplied with additional energy, as by the penetrating missile, plastic and shock waves rapidly reduce to ordinary elastic waves as the pressure behind the wave front falls. Spherical or expanding waves attenuate as they propagate, since their energy is distributed over increasing areas.

EFFECTS OF WAVES IN STACKED PLATES

The first effect of the missile's impact on the top plate is to produce an indentation or depression in the plate. Immediately following indentation and the resulting spherical shock wave emanating from it, a lateral compression and circular bulging about the impact area is brought about by the reflection of the spherical shock wave at the upper free boundary. As the intensity of the shock wave that sweeps over the upper free surface rapidly attenuates, the circular bulging vanishes and leaves a simple semi-toroidal protrusion surrounding the area of impact.

The radial mass velocities behind the spherical shock wave induce an expansion of the penetration hole. The centrifugal mass velocity of the expanding (flattening) projectile may be greater than that of the target. It then exerts an added centrifugal pressure on the top layer of the target, superimposing an increased centrifugal pressure along the free surface at the spherical shock front. Material displaced by enlarging the penetration hole thickens the plate around the hole. The shock wave reflecting from the upper surface in the initial stage of perforation also takes care of some of the displaced

material. However, the upward velocity of this material is so high that it creates a semitoroidal bulge that must exceed the needs; the upward velocity can be checked only by some downward traction after the crest of the pulse has passed. This induces a downward velocity of the upper surface of the material that also may exceed the needs, resulting in a fluctuation of the thickness of the plate about its new normal thickness.

Movement of material by the high pressure in the shock wave brings the surfaces at the interface into intimate contact, filling in all asperity gaps by plastic flow. Thus, due to surface irregularities that separated some parts of the surfaces, there is, in a sense, a partial collision of surfaces. The expansion of the spherical shock front results in a spreading area of intimate contact.

As the cavity formed by the penetration of the projectile advances across the interface, impact pressure forcing the superjacent plate into close contact with the subjacent plate is abruptly reversed in the area immediately surrounding the puncture. It is postulated that this reversal of pressure is due to the blowback of material ejected from the expanding crater in the subjacent plate and to the shock pressure in the superjacent plate. The blowback effect is caused by the mass velocity behind the relief wave. Material having kinetic energy in excess of its cohesive strength is ejected. The result resembles that of an explosion, a possibility that can by no means be completely excluded, since energy distribution curves and the brilliance of the impact flash support the possible existence of a vapor phase.

As the impact cavity moves into the subjacent plate, the deformation bears a considerable resemblance to that in the superjacent plate. The plate tends to thicken in the region surrounding the cavity and to develop an annular bulging of the surface in that region.

When part of a plate has been deformed by the passage of a shock wave, while in the rest of the plate the intensity of the wave has subsided to elastic levels, severe constraints are left in the affected parts. The parts that have been shock-deformed do not return to their original shapes, but the parts that were merely elastically deformed normally would, if they were not prevented from doing so by the fact that they are joined to the part that has been permanently deformed. This leaves important residual stresses and strains in the plate, as an equilibrium compromise is reached, in which the residual compressive stresses in the shocked material are in equilibrium against new stresses and strains that are set up in the remainder of the plates. Such stresses are of the static type and remain present after the body has come to rest.

Superposed on these are thermal stresses produced by the varying temperatures in different parts of the plate. Usually the hotter parts are under compression because they were expanded by the higher temperature, while the parts that are at a lower temperature usually are under tensile stresses. Such stresses are ephemeral and disappear as the body assumes an even temperature. Except for a few materials such as glass, the stresses are not important enough to be of any consequence.

There are stresses from the bending, twisting, and other large-scale deformations set up in the body as a result of momenta transmitted to parts of the plate and the inertia of the remainder of the plate to which such momenta have not been delivered. Such stresses may produce permanent deformations, fractures or, when their energy is low, simply a periodic vibration resulting in acoustic waves in the surrounding atmosphere.

EXPERIMENT

GENERAL DISCUSSION OF WELDING

Welding is the joining of metal surfaces to form a single integrated whole. A weld is obtained when materials at the surfaces to be joined are able to form new crystals that extend and interlock across the interface. Welding is inhibited by layers of adsorbed atmospheric gases and other surface impurities that present a chemical hindrance to union across the interface, and also by applied energy levels too low to activate the atoms.

A surface that is free from inhibiting surface layers, such as the surfaces of a fresh fracture, can only exist for a brief instant of time in the normal atmosphere of our earth environment. These surface layers are composed of molecules of atmospheric gases that are attracted to the surface, reaction products of the surface material and atmospheric gases, such as oxides and nitrides, as well as miscellaneous substances that may find their way to the surface. Except in those cases where we wish to weld two surfaces, these surface layers are very useful. (Evaporation of layers of surface impurities including lubricants from bearing surfaces in the vacuum of space, with the probability that the surfaces will then weld or "freeze," is a serious problem in the design of space equipment.)

Successful welding techniques dispose of any weld-inhibiting layers either by destroying their continuity or by causing them to be absorbed or mixed into material behind the surface. In resistance welding, the surface layers are absorbed into the melt. In friction welding, friction at the surface destroys the continuity of the inhibiting layers and the exposed atoms react across the interface. The blacksmith of former times usually cut on a bias the material to be joined. The peening or hammering sent stress waves along the interface that tended to fracture the layers between interfaces and bring the atoms into intimate contact.

In hypervelocity impact welding and in contact explosive welding, the disturbance racing along an interface forms a rippled interface. This increases the surface area at the interface, shattering and opening wide fissures in the weld-inhibiting surface layers. The high pressures and turbulence associated with such disturbances promote mixing and intimate contact of materials across the interface. In the standoff technique of explosive welding, which involves the application of pressure normal to the interface, it should be necessary to employ very high pressures to achieve the same results.

SPOT WELDING BY HYPERVELOCITY IMPACT

In the experiment described below, we observed conditions under which the localized impact surfaces of two metal plates underwent severe plastic deformations and were forced to jet into the minute space between the plates. This surface jetting in the space ahead of the impact point or other relative lateral motion serves to remove or disrupt the omnipresent surface oxide film, aids in the diffusion of the metal atoms across the interface by straining the surfaces at a very high rate, and forms a wave-like or rippled surface that increases the area of intimate contact and enhances interlock. The interaction between the jets from the two surfaces, followed by an almost instantaneous release of load, permanently bonds the two metal plates.

Three plates of 1100 aluminum in the 0 temper, each plate 0.020 in. thick, were bonded together in the flush position and subjected to normal impact by a hypervelocity plastic disc. Projectile mass was approximately 1/2 mg and impact velocities ranged from 21,000 to 26,000 ft/sec^{-1}. An exploding foil gun[9] was used to accelerate the Mylar projectile.

Figure 1 shows the damage resulting from particle impact: a hole with the customary lip in the first plate, a crater in the second plate, and slight bulging of the second and third plates. The material surrounding the hole in Plate 1 was peeled back (in a manner typical of this type of impact), so that a small separation gap existed in a localized region between the first two plates. Plates 2 and 3 were undoubtedly spot-welded together. They could not be separated by simple mechanical means, and metallurgical examination provided additional proof. Knoop microhardness data were obtained at various locations on the impacted plates and the observed values are shown at the location of the hardness determinations as callouts in the figures. Figures 2 and 3 are photomicrographs of the spot-welded area. A periodic wave-like structure in the bonded zone can be seen in Figure 2. However, the waves do not extend over the entire mating surface of Plates 2 and 3, and a smooth-welded zone beneath the impact crater can be seen in Figure 3. The discontinuity observed indicates that the jet flow of material is unstable. This result is not unexpected. It should be observed that an essential difference between sheet jets and the more familiar jets from cones is the convergence of conical waves toward the axis of the cone jet.

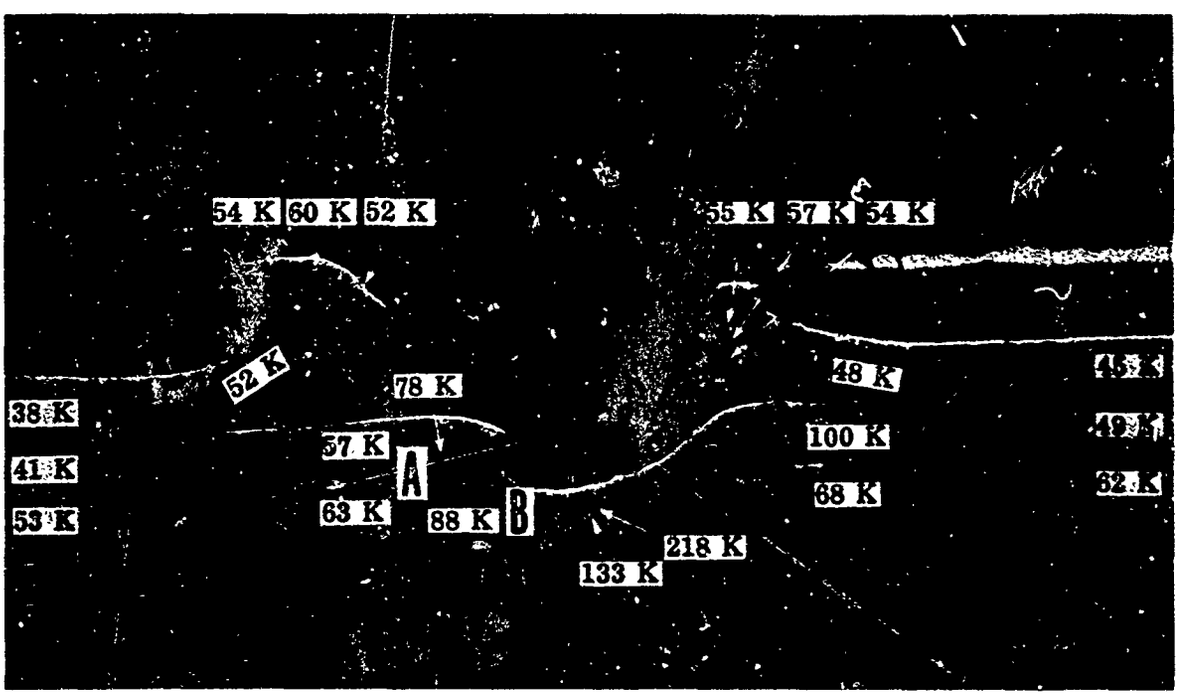

Figure 1. Damage Sustained From Impact of a Milligram Particle at 21,800 ft/sec^{-1} Velocity (numbers indicate Knoop hardness)

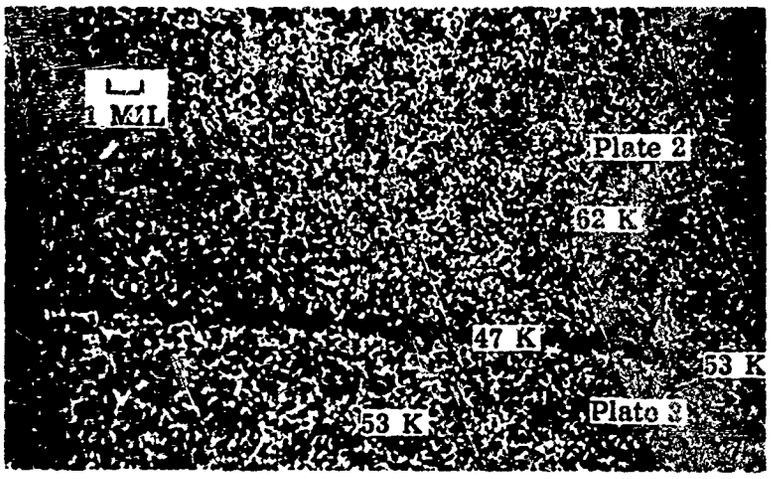

Figure 2. Wave-Like Structure at the Interface of 1100-0 Aluminum Plates; see A of Figure 1 (numbers indicate Knoop hardness)

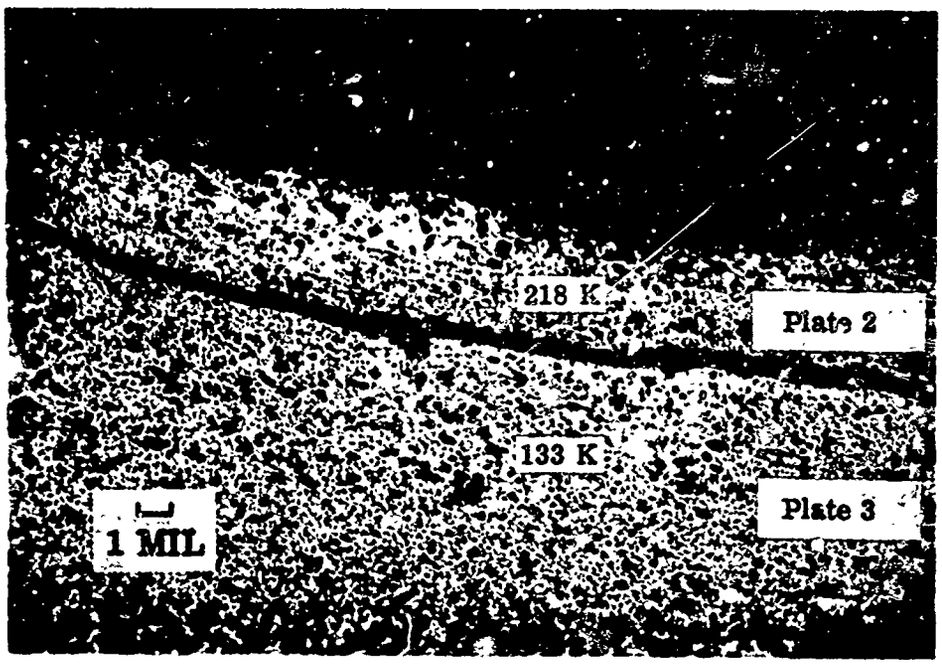

Figure 3. Interface Beneath the Crater; see B of Figure 1 (numbers indicate Knoop hardness)

Impact of the projectile with the three-plate system produced high pressure and shear (contact pressure of ~4 x 10^6 psi) in the extremely localized area of the impact. These stresses are considerably greater than the dynamic yield stress of the 1100-0 aluminum; therefore the metal can be treated as a fluid. The stress field in the region of impact will be composed of a high hydrostatic pressure with the relatively small shear stresses usually observed in fluids of low viscosity. The motion in the impact area can be considered a problem in fluid dynamics and has been treated [6, 10] by the classical hydrodynamics of a compressible perfect fluid. Equations describing the flow were obtained and three flow patterns are possible: (1) subsonic jet velocities, (2) supersonic jet velocities at angles of incidence less than a certain critical value, and (3) supersonic jet velocities at angles of incidence greater than the critical value. [1, 6] The important result to note is that a forward stream of material — a jet — is predicted. No jet occurs when a very small contact angle is used and no wave-like structure is observed at the interface (Figure 3); larger contact angles produce wavy joining. Presumably, the jet speed decreases and the jet mass increases as the effective angle between particle velocity vectors in the two shock-deformed plates becomes greater than the critical angle. [6]

Assuming that the two metal plates behave as nonviscous compressible fluids, we can then consider the impact collision as the movement and impact of two free jets, representing the two plates. Motion is referred to a coordinate system in which the instantaneous point of collision P is stationary (Figure 4). The value of the stagnation pressure at P can be obtained from Bernoulli's equation for steady compressible flow by using an approximate isentropic compression curve obtained from measured Hugoniot curves. From the stagnation point, the inner part of each plate flows forward; the inner fluid layer divides around the stagnation point, with part contributing to the jet and the remainder to the slug. Thus, material from Plates 2 and 3 first comes into contact at the stagnation point, inside the metal, where the pressure is extremely high (maximum at the stagnation point) and where maximum shear is encountered. The surface jetting of the stream from one plate divides against the stream from the other, and flow around a deformable or fluid base provides a condition conducive to the periodic formation of oscillations. Any fluctuation in the Fuchs shocks [6] extending from the junction of the two streams appears to start an oscillation that produces periodic forms such as the wavy joining shown in Figure 2. Abrahamson [5] examined such oscillations in a single fluid stream (water) dividing against a deformable base (silicone putty).

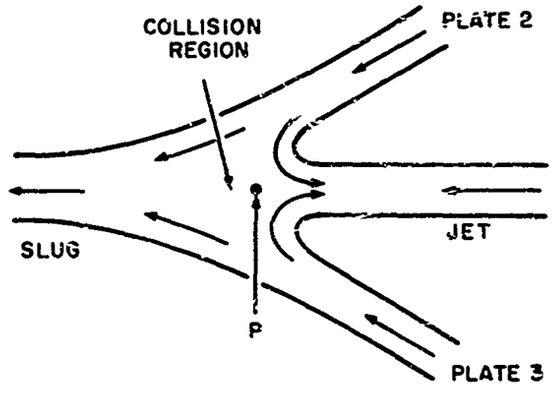

Figure 4. Symmetric Collision of Two Plates; after Walsh et al. [6] (Motion is referred to a coordinate system in which the instantaneous point P is stationary)

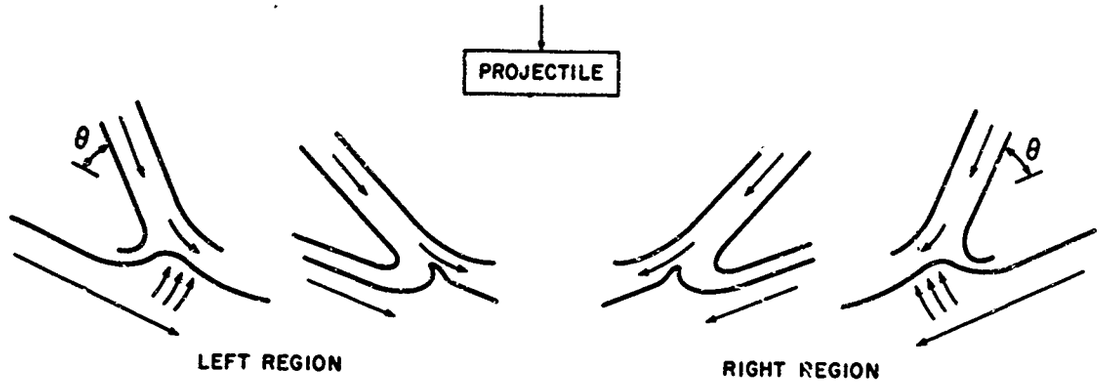

a. Schematic of Crest Direction in the Wave

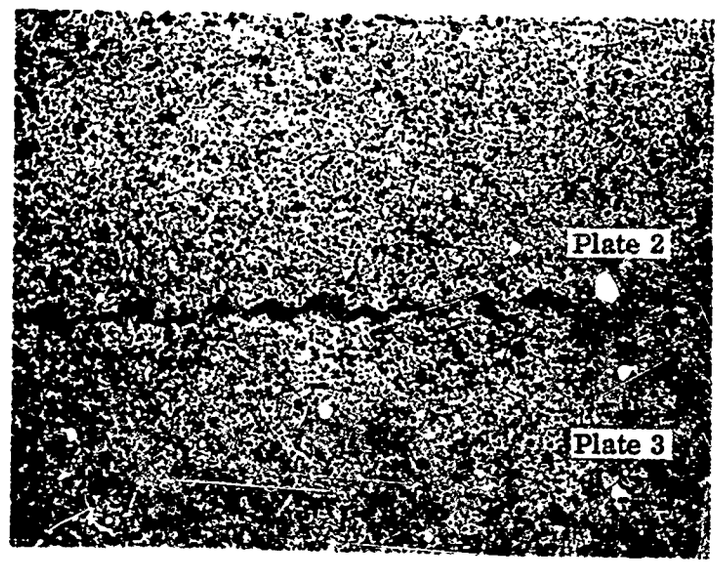

b. Closeup View of Wave Form to Right of Crater

Figure 5. Wave Direction

The wave structure is observed on both sides of the deformed area but not at the base region. Moreover, the wave structures at opposite positions on the deformed surface appear to be identical in shape, except that they are mirror images. A cross section of the target system shows that the crests of the waves to the right of the bottom region are turned to the right; those to the left of the bottom are turned to the left, as indicated in Figure 5a. Figure 5b shows a closeup view of the wave form in the right weld region (see Figure 2 for wave structure in the left weld region). This behavior of the crests indicates that the velocity of the base plate was somewhat higher than that of the second plate. It is not yet possible to provide an unequivocal solution to this problem nor to establish the value of the critical contact angle, since the results of the flow are not well known. However, the results in the figures are in qualitative agreement with a plausible extension to the present case of the considerations in the references.

RIPPLE FORMATION WITHOUT WELDING

Rippled surfaces have been produced on metal plates with projectiles that are harder (steel) and softer (Mylar) than the target, and the same (aluminum) as the target. When the superjacent plate is thin (about 0.23 cm of 6061-T6 aluminum for an impact energy of about 10^{10} ergs) and the subjacent or backup plate is thick, the superjacent plate will be petalled outward as shown in Figure 6. Examination of the petals reveals that they were formed in shear and that each petal possesses a series of transverse ridges (Figure 7). The subjacent plate, being thick, is able to withstand the impact loading without bending. There is, however, an appreciable thickening of the plate extending outward from the impact cavity to a distance of nearly twice the cavity radius. About halfway between the cavity and the boundary of the thickened section is the outer radius of a circular ring where the surface of the metal has been rubbed, and a typical ring of galled material is shown (see Figures 6 and 8). This ring on a bright aluminum or magnesium surface appears to be somewhat darker than the remainder of the surface. On the surface of this darker ring of material are ripples or ridges concentric to the cavity.

When the superjacent plate is thicker than that described above (about 0.48 cm of aluminum for the same impact energy) and the subjacent plate is thick, both plates around the cavity are deformed away from the interface. The dark ring and the pattern of concentric ripples appear on both surfaces of the former interface and are mirror images. When a number of thin plates are impacted, the deformation becomes more complex.

This structure of ripples, concentric to the impact cavity, without welds has been produced in stacks of two 6061-T6 aluminum plates (the bottom plates were 0.7 to 1.9 cm thick and the superjacent plates either 0.23 or 48 cm thick) and in all four mating surfaces of a stack of three HK 31A magnesium plates (each 0.635 cm thick). In these experiments the energy was delivered in air by a 0.55 g steel cylindrical projectile (length/diameter ratio 0.357) at impact energies from 2.26×10^{10} to 7.8×10^{10} ergs. In all cases where the rippled surfaces were observed, the diameters of the cavities produced in the targets were substantially larger than the initial diameters of the projectiles.[11]

A ripple pattern was not produced in stacks of 6061-T6 aluminum plates punctured in steel-jacketed military-type .30 caliber bullets at about 914 m/sec in air (impact energies of about 4×10^{10} ergs). The diameters of the punctures were the same as the diameters of the bullets. Cutting off the bullets behind the ogive (a right circular cylindrical projectile) prior to firing (mass and velocity not measured) altered the shape of the cavity but did not produce a rippled pattern.

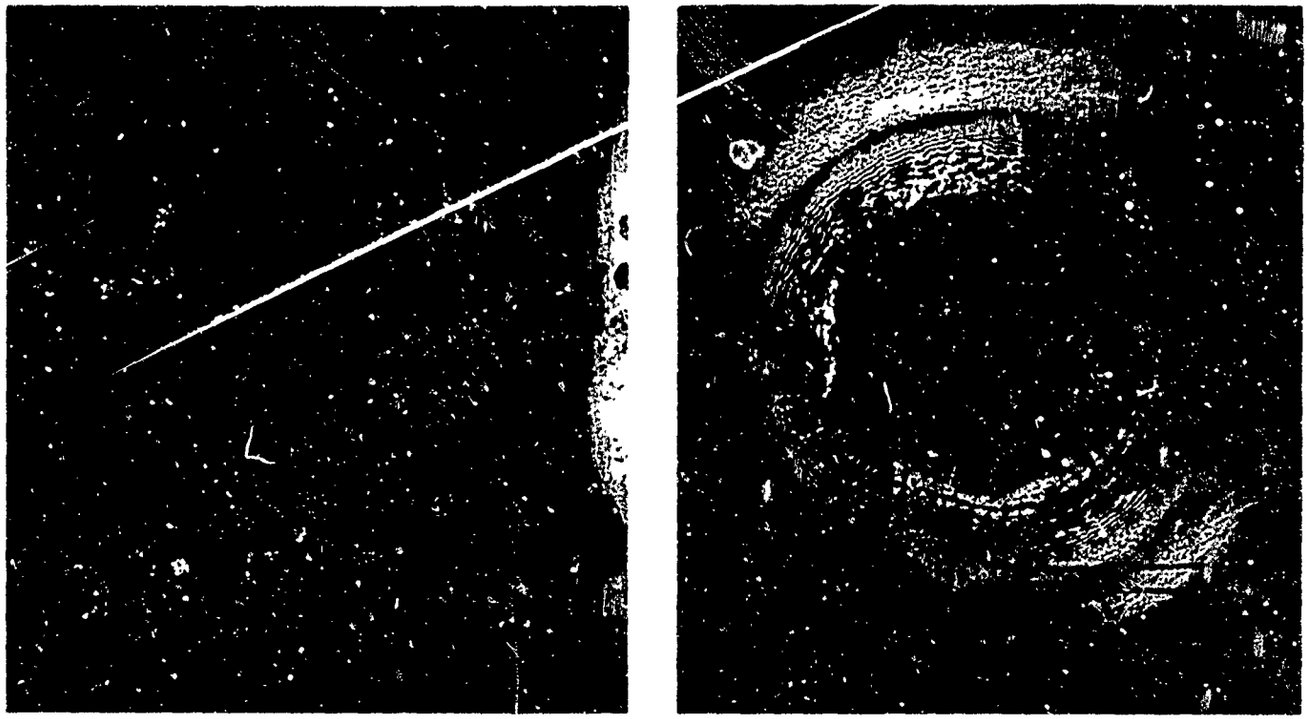

a. Superjacent Plate

b. Subjacent Plate

Figure 6. Impact Effect on Stack of Two Plates in Contact (A indicates the outer edge of the ripples; B, the outer edge of the galled ring; and C, the outer edge of thickened section of the plate)

Figure 7. Transverse Ridges on Petal Surface of Superjacent Plate

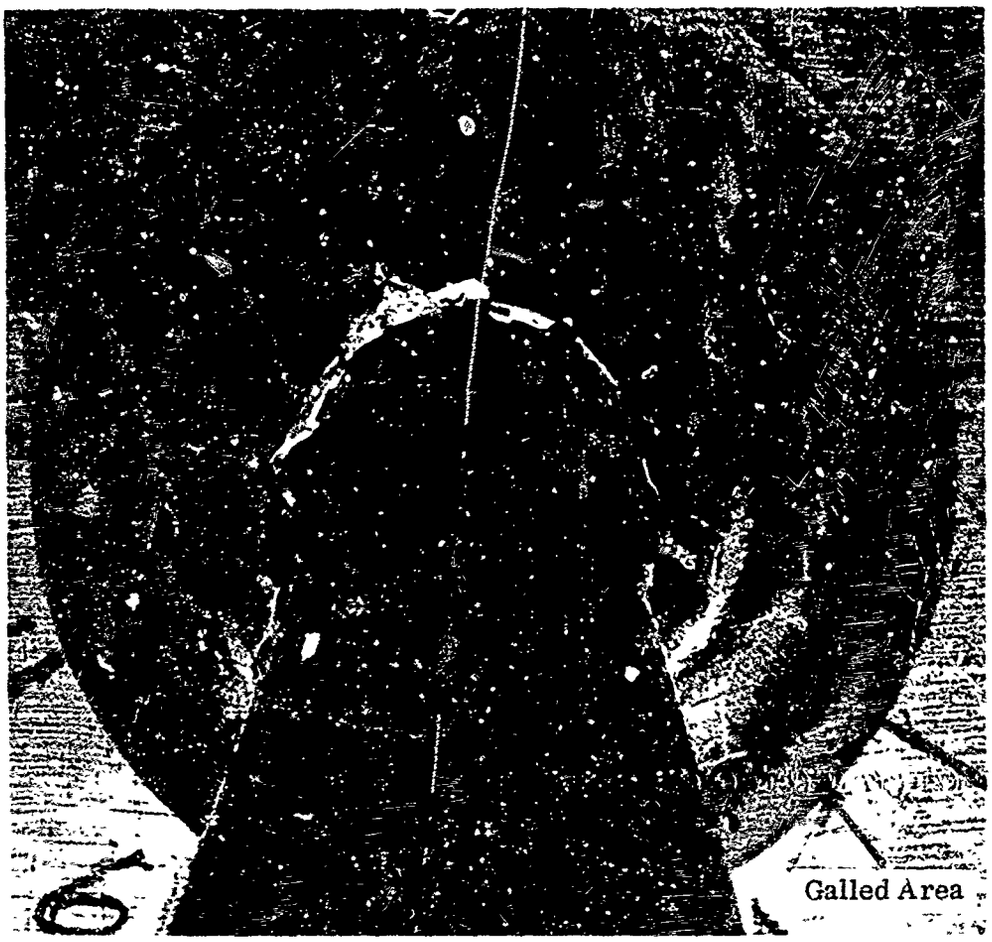

Figure 8. Mating Surface of a Plate After Impact

The results of a number of experiments using .220 Swift and 7.62 Mauser rifles with special loads in air are pertinent. Rippled structures without welding were produced on 6061-T6 aluminum plates having superjacent plates 0.23 cm thick by impacts of 0.25 g aluminum balls with energies of about 5.7×10^9 ergs (estimated from a comparison of powder charge, mass, and velocity measurements with identical experiments in vacuum). Conditions for the formation of these ripple patterns are believed to be threshold for the materials combinations. Slightly larger aluminum balls whose velocities were about 600 m/sec slower than the 0.25 g balls did not produce such ripples around the cavities.

It appears that there is a threshold impact energy below which the patterns are not produced, but that the characteristics of projectile expansion on impact and energy densities are also factors.

Ripple patterns on the superjacent surfaces are more distinct than those on the subjacent surfaces. The patterns are not perfectly symmetrical but appear to be affected, for example, by surface irregularities. There is a very slight tendency for

the ripples to align themselves with the large surface irregularities (surface rolling texture) produced by rolling out or sizing sheet stock. A scratch or a rolling groove across one of the mating surfaces will be reproduced in raised relief on the opposite surface but only on that part of the surface where the ripples occur (Figure 9). The total impact energy available is sufficient for such work (the work to emboss) only if the stresses are transient and highly localized.

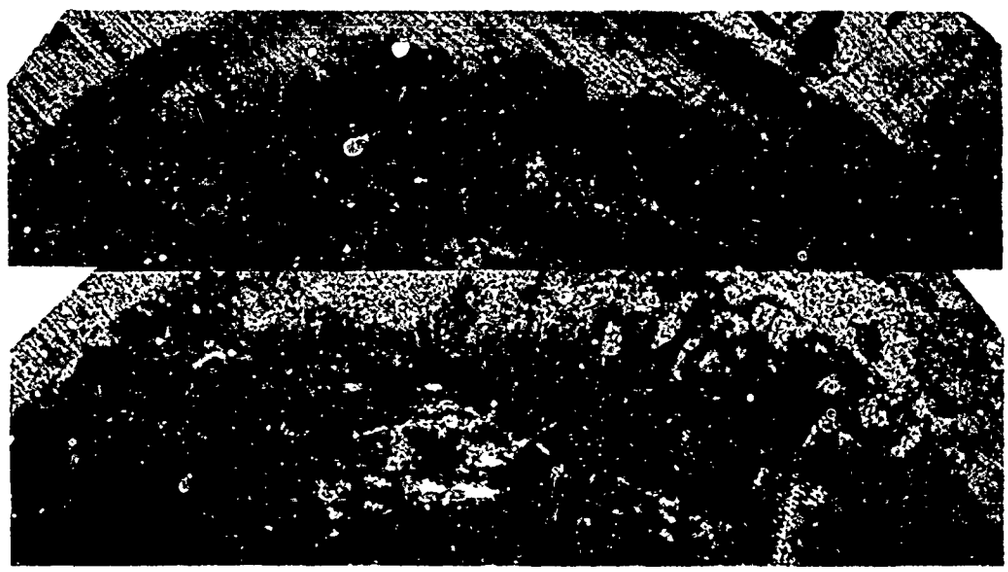

Figure 9. Reproduction of a Scratch (upper figure) on Mating Surface (lower figure) in Raised Relief. (The upper figure is printed reversed for comparison with the lower figure)

In one experiment there was a tilt in the right circular cylindrical projectile at the instant of impact, and the unsymmetrical impact orientation resulted in an unsymmetrical pattern of ripples. The ripples in the direction in which the impact force was inverted by this orientation, in this instance, measure a greater distance from crest to crest, have a greater amplitude, and extend farther outward toward the outer edge of the darkened ring than do the ripples on the opposite side (Figures 6 and 8). Allen et al.[1] and Abrahamson[5] observed that similar changes occurred in the ripples produced on the surfaces of cylindrical and conical projectiles impacting metal plates. They attributed these changes to a variation of the impact angle.

Measured distances from crest to crest of the ripples produced with several target configurations have varied from 0.020 to 0.305 mm; amplitudes, from 0.01 to 0 068 mm. The usual ratio of amplitude to distance from crest to crest is close to 0.25 for systems that were not welded, while the ratio for profiles where bonding occurred is higher with an upper limit in excess of 0.5.

In one cross section of the second plate of a magnesium target, at a point outward from the cavity to the first distinct crest and measuring outward, the distance between crests was 0.084 mm. At the position of the crest for ripple number eleven, the distance between crests had increased to 0.102 mm. The distances remained close to this figure out to the crest for ripple number twenty-six, where the distance decreased again to 0.084 mm. After the crest for ripple number forty-three, the ripple pattern disappeared for a distance of 0.625 mm. The surface beyond the 0.625-mm gap was

marked by eight additional ripples that were 0.076 mm from crest to crest. The portion of the metal plate where this rippled surface structure was found was only moderately deformed, with a gentle convex curvature downward due to the hole punched in the three-plate system by the hypervelocity projectile. The surface of the contacting plate was a mirror image of the surface with the intermittent ripple pattern.

Within any one series of measurements along the radius for a plate that was rippled but not greatly distorted (bent) and not welded, the distances from crest to crest and the amplitudes appear to be fairly uniform except for distortions introduced in the surface after the formation of the ripples. There are, of course, rather large variations in such measurements when the dimensions of the plate have been distorted by the mechanics of the impact after formation of the concentric ripple pattern. A persistent tendency for measurements between crests, at the outer and inner boundaries of severely deformed plates (Figure 6), to be smaller than those in the center is probably real and not entirely a result of surface distortions.

The frequency computed by dividing the velocity of shock-wave propagation by the measured distance from crest to crest in the ripple pattern is on the order of 10^7 cps. Since the computed shock velocity will change with shock intensity and temperature, and the bulk modulus is unlikely to be constant at very high pressures, the equations can only be very approximate. The foregoing estimate of frequency is, therefore, for an order of magnitude only.

If the mating surfaces have remained reasonably flat after impact, both the blackened ring and the ripple pattern of the mating surfaces can be matched; i.e., they are mirror images. Mating surfaces that have been severely curved (deformed) by the impact often give the appearance of being mirror images, but they do not match dimensionally. Where bonding or welding has occurred, however, the ripples mesh, so that an interlocking structure is formed. These ripples frequently show a deformation as if there had been a very slight relative movement of surfaces coincidental with or immediately following their formation. These circumstances are indications that the ripples were formed before severe deformation of the plates had occurred.

This observation, we believe, affords proof that the ripples were formed before the "severe" deformation of the flat plate geometry. The result is expected since it is the passage of the collision site that generates the ripples, and it is the high mass velocities behind the shock waves induced by this collision that eventually produce the large changes in geometry.

Some of the ripples on plates that were not welded have a sawtooth structure with sharp peaks. These have been observed at interfaces that apparently were welded or partially welded, but were broken or pulled apart by the shock dynamics of the plate system (Figure 10). The genesis of the ripples and their form does not appear to depend upon geometry, since plate thicknesses involved vary from 0.025 to 0.625 cm without correlation of thickness to ripple structure. Hence, reflections of translational energy at an outer surface of a superjacent plate is probably not important.

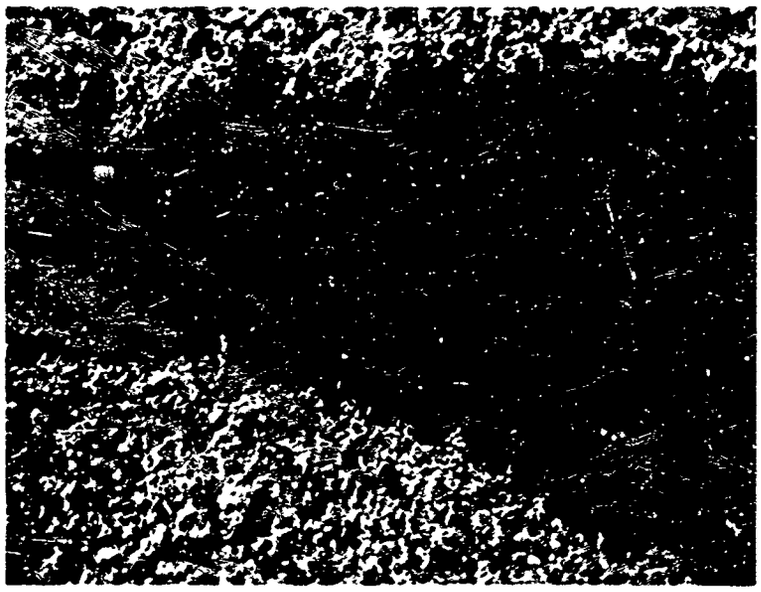

Figure 10. Sawtooth Structure of Ripples

RIPPLE FORMATION WITH WELDING

During the spot-welding experiments we discovered by metallographic examination of the cross section of the weld that the structure was rippled. The ripples showed a definite crest structure, which may explain the mode of their formation; that is, the movement of the plastic surfaces at different velocities while the surfaces are held together under the high pressure produced by the projectile impact. As indicated previously, the ripple effect associated with the welding may be described as "surface jetting," which enhances welding because of the maximum surface friction and the increased contact area at the interface.

Phenomena Observed from Experiment

Hypervelocity particle impact welding was obtained by firing 0.005 g Mylar cylinders into stacked targets of aluminum or copper plates, or a combination of aluminum and copper plates. In one experiment, a target of 1100-0 aluminum plates alternating in thicknesses of 0.064 and 0.010 in. was impacted in vacuum by a Mylar projectile at a measured velocity of 28,200 ft/sec. A cross section of this target is shown in Figure 11a. Welds were produced between the third (0.064 in. thick) and fourth (0.010 in. thick) plates and between the fourth and the fifth (0.064 in. thick) plates. The wavy or rippled interfaces of these welds, shown in Figure 11b, have been attributed to the surface jetting phenomenon previously described.

Permanent welding did not always occur during hypervelocity impact on a stack of plates. In some experiments the rippled interface and weld were produced, but the weld bond was ruptured by shock in the parent metal plates, and the plates became separated. This forceful separation of a once smooth, rippled, and welded structure resulted in a sawtooth and free surface, as seen in Figure 12. In other experiments, either a weld did not form or it was exceptionally weak, but the mating surfaces (plastic and moving at different velocities) were left with the rippled surface shown in Figure 13.

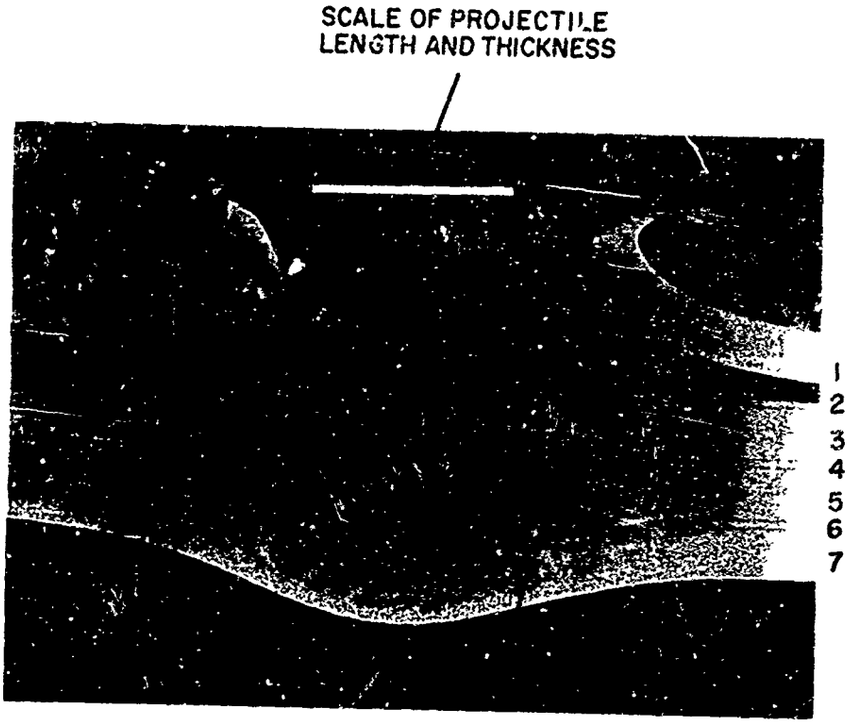

a. Cross Section of Welded Plates

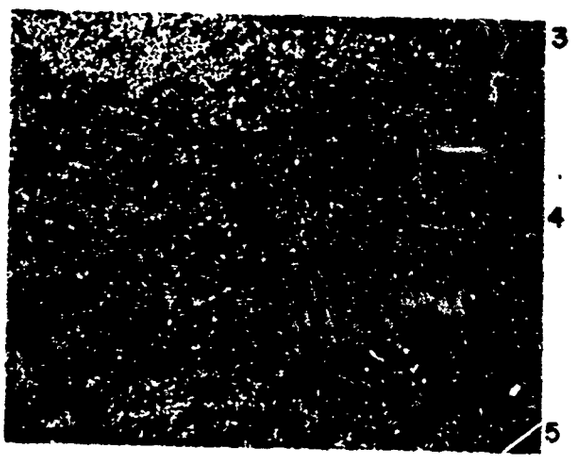

b. Enlargement of Area at Arrow Shown Above

Figure 11. Welded 1100-0 Aluminum Plates (28, 200 ft/sec impact velocity)

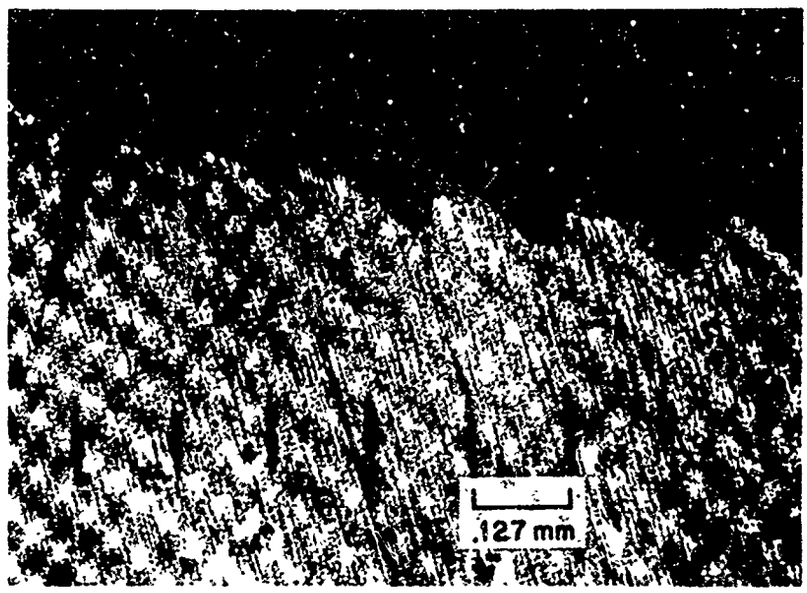

Figure 12. Sawtooth Structure Produced by Forceful Separation of Welded Plates

Figure 13. Second, or Bottom, Plate of Two-Plate Aluminum Target Impacted at 15,000 ft/sec by Steel Cylinder, Showing Concentric Ripples (A), Galled Ring (B), and Distorted Surface (C) Referred to in Figure 14.

The target shown in Figure 13 consisted of two plates — a 0.090 in. thick plate of 6061-T6 aluminum in contact with a 0.375 in. thick plate of the same material. It was impacted in air at 15,000 ft/sec by a 0.25 in. diameter right circular steel cylinder of 0.5 g mass. Figure 14 is a diagram of the sequence of events that we believe occurred during impact upon the target in Figure 13, which punctured the two-plate target system and produced concentric ripples around the puncture. In Figures 13 and 14 we designate the outer boundary of a series of concentric ripples as A; the outer boundary of a galled or chaffed ring-shaped area (evidently caused by relative motion of the two surfaces while they were tightly compressed) as B; and the outer edge of the upward bulge of the surface produced by lateral displacement of material surrounding the puncture as C.

The outer radius of the chaffed ring (B of Figure 13) in a two-plate system, by our hypothesis, should be a measure of the time for penetration of the first plate according to the following relation:

$$R_r - R_p = f(V_\omega,\ T,\ E,\ V_p)\ ,$$

where

R_r = outer radius of the chaffed ring

R_p = radius of the projectile on impact

V_ω = wave velocity

T = thickness of the first plate

E = elastic recoil of the first plate

V_p = velocity of penetration.

Data to establish the functional relation are lacking. However, the available data do show that the outer radius of the galled ring is a function of the thickness of the first plate and an inverse function of impact velocity. This has been determined not only from the experiment shown in Figure 13, but also from two similar ones at different velocities (Table 1).

TABLE 1

SIZE DEPENDENCE OF CHAFFED RING ON IMPACT VELOCITY AND THICKNESS OF FIRST (TOP) PLATE

Measured Impact Velocity (ft/sec)	Thickness of First Plate (in.)	Radius of Chaffed Ring (B of Figure 13) (in.)
9,400	0.090	0.55
15,000	0.090	0.53
14,700	0.1875	0.578

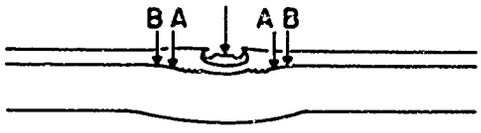

A shock wave in the first plate from lateral pressure of the projectile reduces to an elastic wave at A, the outer boundary of the ripple pattern.

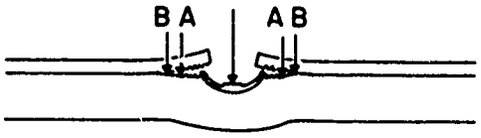

The elastic wave reaches B, the outer boundary of the galled ring, as the projectile punctures the first plate. The pressure holding the plates in contact is reversed by elastic rebound and ejecta now moving from the developing crater in the second plate.

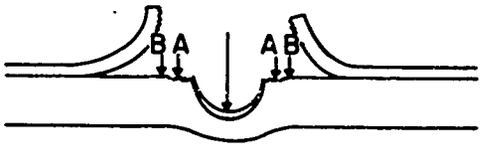

The first plate "petals" under pressure of ejecta from the second plate. Lateral plastic and shock waves are set up in the second plate.

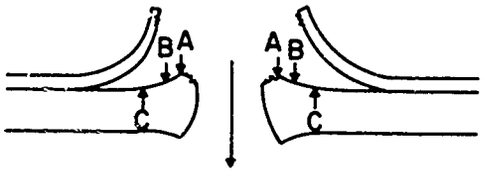

The lateral elastic wave reaches C, the outer edge of the upward bulge of the surface as the second plate is punctured.

Figure 14. Puncture of a Two-Plate System (second plate is shown in Figure 13)

We postulate that the ripple structure in Figure 13 resulted from dynamic instability of the shock wave in the first (top) plate at the interface of the two plates. Material in the first plate was being forced outward radially. The chaffing or galling in the area between A and B was caused by the same shock wave after it had been reduced to an elastic wave. The welling up of the surface, which extends from B to C, resulted from shock and plastic waves produced in the second (bottom) plate during its puncture. The area between B and C is not related to the rippled or the galled area since the surfaces of the first and the second plates were no longer in close contact. The first plate was forced away from the second plate, and deformed in a direction opposite that of the projectile movement, through the force exerted by the relief wave sweeping over the upper free surface of the first plate, by the ejecta from the crater in the second plate, and to a lesser extent by its elastic reaction to the release of impact pressure. No evidence of welding was noted in this experiment, although the same rippled structure is associated with welding.

In some stacked targets, welding has been observed to occur between the first and second plates of the structure and in successive plate interfaces; in other targets the welds did not occur before the second plate and third plate interface. If either the relief wave or crater ejecta (from the projectile and the second and successive layers) force the first plate away from the structure, then a criterion for the welds to occur in this first interface must be the tensile strength of the first plate material. A high ultimate tensile strength material (6061-T6 or 2024-T3) will resist this upward deformation and therefore may enhance the conditions for weldment. On the other hand, a low strength material (1100-0), being more ductile, may easily deform and tear the interlocked ripple crests and form sawteeth.

Mechanism of Impact Welding

The impact energy in the experiment referred to in Figure 11 was 1.85×10^9 ergs. Complete deceleration of the projectile was accomplished in 0.8475 cm, giving a force of 2.185×10^9 dynes. A circle with a radius of 0.565 cm will include the welds, which yields a surface area of 1 sq cm. If we assume that the entire impact pressure was applied normal to the target face simultaneously and was evenly distributed over 1 sq cm, the pressure would be 2.185×10^9 dynes/cm^2 (or 31,750 psi), a direct pressure which we believe to be far below the threshold necessary for welding. The very high pressure contained within the thin expanding circle at the shockwave front must have caused the welding that occurred.*

The impact pressure at the surfaces of a two-plate target system forces the target interface surfaces into intimate contact during the time the projectile is moving through the first plate. At this same time, the projectile and the target material directly under the point of impact expands radially and exerts a lateral thrust (cavitation), tending to enlarge the hole in the first plate. The lateral disturbance is propagated as a shock wave. To permit sufficient heat transfer to induce all parts of the shock wave to propagate at the same velocity, the whole wave front must be very thin, or "steep." Material in this shock front is highly compressed. The high-pressure wave front sweeping radially outward in the first plate can act across the interface, since the surfaces of the two plates are in intimate contact. The inertia of the materials respond-

*A shock wave also results in an embossed surface. On p. 17 we showed that a scratch placed across the surface of one plate is observed in raised relief in the mating face. This reproduction of the scratch did not extend into the elastic region; i.e., not in the region of BC of Figure 13.

ing to the pressure across the interface creates a dynamic instability in the pressure at the interface because of the alternation of jetting and nonjetting collisions. This may cause a rippling of the surfaces as the shock wave sweeps outward.

The rippling of the surface structure increases the surface area and produces maximum shear, which opens wide fissures in the surface layers of adsorbed gases, reactants, and foreign materials. This dilution and shear effect, combined with the induced turbulence and the high pressures within the wave front, promotes intimate contact and permits the linking of metal atoms across the interface. If the surfaces are reasonably free of foreign substances and entrapped air, mate well, and are held in firm contact, then bonding may result. This bonding may be enhanced by an interlocking action of the ripples.

DISCUSSION AND CONCLUSIONS

We have shown that the hypervelocity impact of a Mylar projectile on an aluminum or copper target produced rippled surfaces with welding. In additional experiments, stacks of thin aluminum plates, 0.025 to 0.163 cm thick, and high-conductivity oxygen-free copper plates, 0.075 to 0.163 cm thick, were impacted in partial vacuum using 0.005 g Mylar discs at impact energies from 1.1 to 1.84 x 10^9 ergs. Spot welds were observed in association with rippled interfaces when the targets were sectioned for metallographic examination (Figure 15). These welds were formed between aluminum and aluminum, and between copper and copper. Spot welding also occurred between aluminum and copper, but the bonds were weak and ruptured in the aluminum parent metal. The materials used in these welding experiments are summarized in Table 2. Measurements of the height and distance between ripples, observed from typical metallurgical specimens (Figure 15), are given in Table 3.

Not all surfaces contain well defined ripples. The variations in the ripples are shown in Figure 16. These differences have been attributed to the relative difference in motion of the two plates forming the interface.

The structures of the ripples produced in a stack of metal plates by hypervelocity particle impact, in those formed on the surfaces of projectiles striking thin plate targets at oblique angles, and in those that result from explosively projecting thin plates together at angles oblique to their impacting surfaces are similar enough to justify the conclusion that all ripples have their genesis from the same types of forces and interactions. The circumstances surrounding their formations, however, are quite different. Analysis to construct a model to explain the origins of these phenomena is complex and difficult except, perhaps, for the hypervelocity impact phenomena that are more amenable to analysis.

No part of the target outside the point of impact is affected by the impact until its position is reached by the stress wave. Therefore, no part of the interface can be galled until it is reached by the stress wave. Galling, however, requires contact with another surface. Since the surfaces separate when cavitation passes the interface, the possibility of further galling is ended, and the outer limit of the galled ring marks the position of the stress wave at the instant the surfaces separated. Galling must be accomplished while cavitation is moving through the superjacent plate.

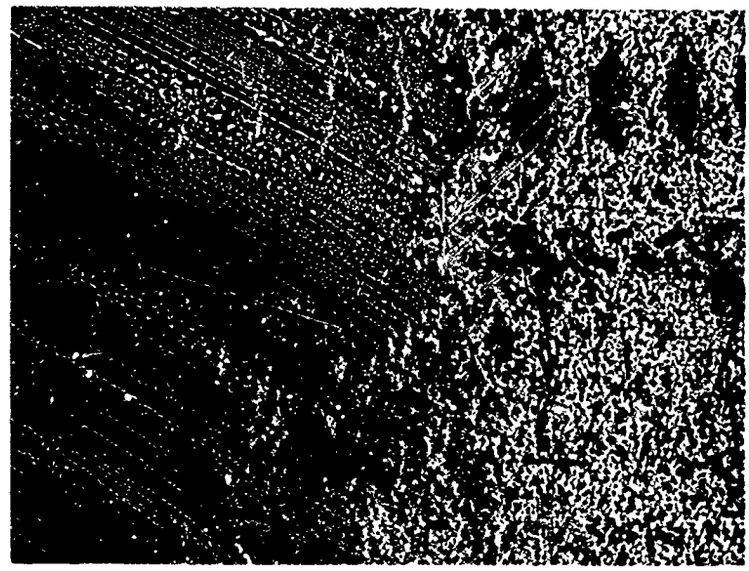

Figure 15. Cross Section of a Spotweld on a Multiplate Target (microhardness indentations are 0.127 mm apart)

TABLE 2

SUMMARY OF IMPACT WELDING EXPERIMENTS

Material	Number of Experiments	Experiments Resulting in Welding
1100-0 Aℓ to 1100-0 Aℓ	10	4
2024-T Aℓ to 2024-T Aℓ	1	0
Cu to Cu	2	2
6061-T4 Aℓ to 2024-T Aℓ	3	0
2024-T Aℓ to 1100-0 Aℓ	4	0
Cu to 1100-0 Aℓ	2	1*
Cu to 2024-T4 Aℓ	1	1*
	23	8

*Weld failed in aluminum

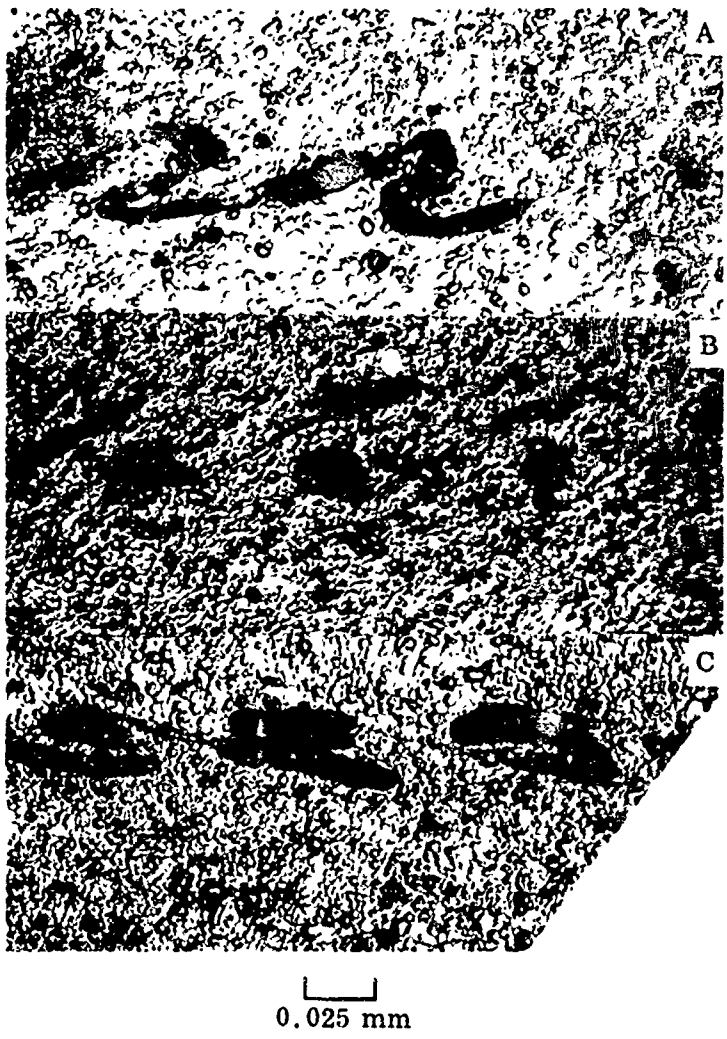

Figure 16. Types of Ripples in Weld at an Interface. (A shows ripples with pointed crests; B, ripples that are not well defined and are beginning to smear out; and C, ripples that are not well defined and are in a later shape of smear-out)

The rippled structure, concentric to the impact cavity and imposed on the surface within the galled ring, is therefore also formed during and simultaneous with the passage of cavitation through the superjacent plate. The process of its formation has to include plastic deformation of the metal surface. [The process of transferring a replica (embossing) in raised relief of the part of a scratch that crosses the rippled structure to the mating surface also requires plastic deformation.] A shock wave is the only source of pressure in the system great enough to cause the material to flow plastically. Therefore the rippled structures are formed during and as a consequence of the passage of the shock wave; i.e., the shock wave supplies the forces that create the ripples. An outer termination of the series of ripples short of the outer rim of the galled ring must mark the decay of the stress wave from predominantly plastic to essentially elastic characteristics.

TABLE 3

MEASUREMENTS OF SERRATED OR RIPPLED STRUCTURES IN WELDED SPECIMENS

Impact No.	Velocity (10^5 cm/sec)	Interface of Plates	Material	Weld	Ripple	
					Distance Between (mm)	Height (mm)
A	8.6	1-2	1100-0 Aℓ	Broken	0.0175	0.01
		2-3	1100-0 Aℓ	Broken	0.073	0.02
		3-4	1100-0 Aℓ	Held	0.088 0.033 0.061	0.025 0.0133 0.033
		4-5	1100-0 Aℓ	Held	0.060	0.020
B	8.35	2-3	Cu OFHC	Held	0.020 0.025	0.008 0.010

The processes of galling require that the surfaces be rubbed together; i.e., there must be a relative motion of one surface with respect to the other. This rubbing could be produced only by the stress wave. If the transfer of stresses across the interface were perfect, the surfaces would move together as a unit and there would be no rubbing. Since there is evidence of rubbing, the transmission of the stress wave across the interface is not perfect and there must be reflections or interferences at the interface.

One possible genesis of the rippled structures that is consistent with vibrations in the range of radio frequencies may be postulated on the basis of reflections from the interface: the incident wave is a hydrodynamic shock wave and is therefore not restricted to sonic velocity as are elastic waves. Since the reflected portion of the wave is moving through material already heated by the incident wave, it will, according to hydrodynamic theory, increase its velocity and catch up, merge with, and reinforce the incident wave forming a Mach stem.[11] The reinforced stem tends to form a ripple or depression in the interface (a ripple with a crest on one plate surface is a ripple with a depression on the other plate surface). This deformation of the interface changes the angle of incidence, causing the reflected portion of the wave to be scattered which abruptly cuts off the reinforcing pressure; the cycle then restarts.

While the use of stress waves to destroy the continuity of weld-inhibiting surface layers during welding has been a practice since antiquity, many of the modern welding practices have tended to obscure the significance of such operations. The possible uses of stress waves for obtaining particular surface effects may be an important means for improving welding techniques. The effectiveness of stress waves for disrupting surface layers is probably greatly enhanced by moderate intersurface friction.

The structures of surface galling and ripples in thin-plate stacked targets are a record left by the stress waves. As such, it appears that they will be of considerable value in studies of hypervelocity cratering.

REFERENCES

1. W.A. Allen, J.M. Mapes, and W.S. Wilson, "An Effect Produced by Oblique Impact of a Cylinder on a Thin Target," J. of Appl. Phys. 25, 675-676 (1954).

2. R.F. Rolsten, H.H. Hunt, and K.H. Meyer, "Deformation and Wave Structure Produced by High-Velocity Impact," J. Appl. Phys. 35 (5), 1655-1956 (1964).

3. J. Pearson, "The Explosive Working of Metals," Paper presented at the National Symposium of the Society of Aircraft Material and Process Engineers, Dayton, Ohio (March 1960).

4. J.S. Rinehart and J. Pearson, The Explosive Working of Metals (New York, N.Y.: Macmillan and Co., 1963) pp. 305-316 and 64-66.

5. G.R. Abrahamson, "Permanent Periodic Surface Deformations Due to a Traveling Jet," J. Appl. Mech. 28, 519-528 (1961).

6. J.M. Walsh, R.G. Shreffler, and R.J. Willig, "Limiting Conditions for Jet Formation in High Velocity Collisions," J. Appl. Phys. 24 (3), 349-359 (1963).

7. G.R. Cowan and A.H. Holtzmann, "Flow Configurations in Colliding Plates: Explosive Bonding," J. Appl. Phys. 34 (4) 928-939 (1963).

8. A.E. Bayce and E.S. Wright, Stanford Research Institute, private communication.

9. R.W. O'Neil, et al., Effects of Hypervelocity Impacts on Materials, Technical Operations Research, AFML-TR-65-14 (January 1965).

10. G. Birkhoff, et al., J. Appl. Phys. 19, 563-582 (1948).

11. Los Alamos Scientific Laboratory, The Effects of Atomic Weapons (Washington, D.C.: U.S. Government Printing Office, 1950), Sections 3.41-3.60.

PART II

METALLURGY OF ALUMINUM INGOTS FOR HYPERVELOCITY IMPACT TARGETS

BACKGROUND AND OBJECTIVES

Impact theory and structural design have generally followed separate paths, and few attempts have been made to integrate theoretical concepts and recognized phenomena in the development of structural systems. The prime prerequisite for the establishment of realistic design criteria is a systematic experimental and theoretical investigation carried out on materials and structural configurations useful in actual vehicle design.

For this program, we initiated a systematic approach combining uncommonly used metallurgical properties of materials with impact theories pertinent to hole and crater formation. The ultimate objective of the program was to establish the modes of energy dissipation in the impact process.

Metallurgical examination of several targets routinely employed in impact studies showed that the sheet stock was not homogeneous; its top and bottom area was a fine-grained or recrystallized structure and its central portion had a preferred orientation of the large crystal grains due to cold work. It is almost impossible to correlate impact damage with materials properties because of the lack of homogeneity in the target. Moreover, targets of this type do not lend themselves to energy partition studies.

Many efforts have been made to relate the extent of impact damage to the properties of the target material. These efforts probably started in 1742 with the resistance-to-penetration theory of Robins. Between 1835 and 1845 the French conducted a series of experiments to measure the velocity of cannonball fragments. The fragment velocity was computed by assuming a constant cratering efficiency, that is, a constant ratio of crater volume to the kinetic energy of the fragment. One of the earliest correlations of cratering data was made by Helie, who observed that the crater volume was approximately proportional to the kinetic energy of the impacting projectile where the constant of proportionality is a function of the target strength.

Cratering by a hypervelocity impact involves shock compression of the target material to very high pressure, and the subsequent motion involves high strain and stress. Although the initial phase of the motion resulting from a high-velocity impact may be adequately described by hydrodynamic principles, as a result of geometrical divergence and dissipation the stresses rapidly decay to the point where material strength becomes important. Pressures operative immediately after impact are clearly not representative for the greater part of the cratering process and cannot serve as a valid basis for neglecting the strength of materials. The bulk of the crater formation is caused by a process of energy dissipation and target deformation, during which time the only restraining forces are the target properties.

It was recently shown[1] that the hypervelocity impact force per crater surface area can be correlated with the ultimate tensile strength when the measured crater dimensions in aluminum are corrected for relaxation. The applicability of the proposed cratering model was extended to include eight aluminum alloys (1100-F, 1100-H14,

2014-T6, 2017-T4, 6061-T6, 7075-0 and 7075-T6) as well as oxygen-free high-conductivity (OFHC) copper. A different strength parameter — the true stress to fracture — was proposed and shown to be applicable.

The goals set forth for this program were to establish:

Short Term

1. Projectile mass
2. Impact crater damage to a target of quasi-infinite thickness
3. Impact spall damage
4. Impact hole damage to thin plates

Long Term

5. Design criteria for flight structures
6. Mechanism of impact with a realistic mathematical model.

With these objectives in mind it was established quickly that the inherent properties of the high-velocity low-mass plastic projectile accelerated with the exploding foil gun could not be used with targets fabricated from ordinary commercial material.

Commercial material or standard mill product metal is not homogeneous in grain size or texture because of its fabrication process. This inhomogeneity is manifested in a test specimen with a rolled texture (Figure 17) with variable mechanical properties. These variables become increasingly significant with the decreasing size of the projectile.

Figure 17. Inhomogeneous Aluminum Target Specimen (dimensions not to scale)

To eliminate the problems associated with an inhomogeneous target material, aluminum ingots of 1100-0, 7075-0, and 7075-T6 were prepared by casting. Each alloy type was handled individually and with the same testing equipment in order to provide the metallurgical data required to characterize the target stock material.

EXPERIMENTAL STUDY

PREPARATION OF INGOTS 1100-0, 7075-0, AND 7075-T6

All ingots were cast by the DC process. The 1100-0 ingot (Figure 18) was 24 in. long, 16-1/2 in. in diameter, weighed 521 lb, and was in the as-cast condition. The size of this ingot and the low concentration of alloying element were the bases for considering annealing unnecessary. Ten ingots (plus one small stub) of 7075-0 (Figure 19), each 24 in. long and 3.4 in. in diameter, with a total weight of 238 lb were annealed for 2 hr at 775°F and still air-cooled. Ten ingots of 7075-T6 (Figure 20), each 24 in. long and 3.4 in. in diameter, with a total weight of 234 lb were solution heat-treated at 870°F for a period of 8 hr, quenched into water at 150°F, and aged for 26 hr at 250°F.

HARDNESS TRAVERSE

Aluminum 1100-0

The cap was removed from the ingot in order to eliminate any end effects. A 1-in. thick slice was removed and the Brinell Hardness Number (BHN) was established by applying a 500-kg load to a 10-mm diameter steel ball for 30 sec. Hardness determinations were made at 1-in. intervals as shown in Figure 21. The hardness value of 24 BHN over a 6-in. radius leaves no doubt about the hardness uniformity of the ingot.

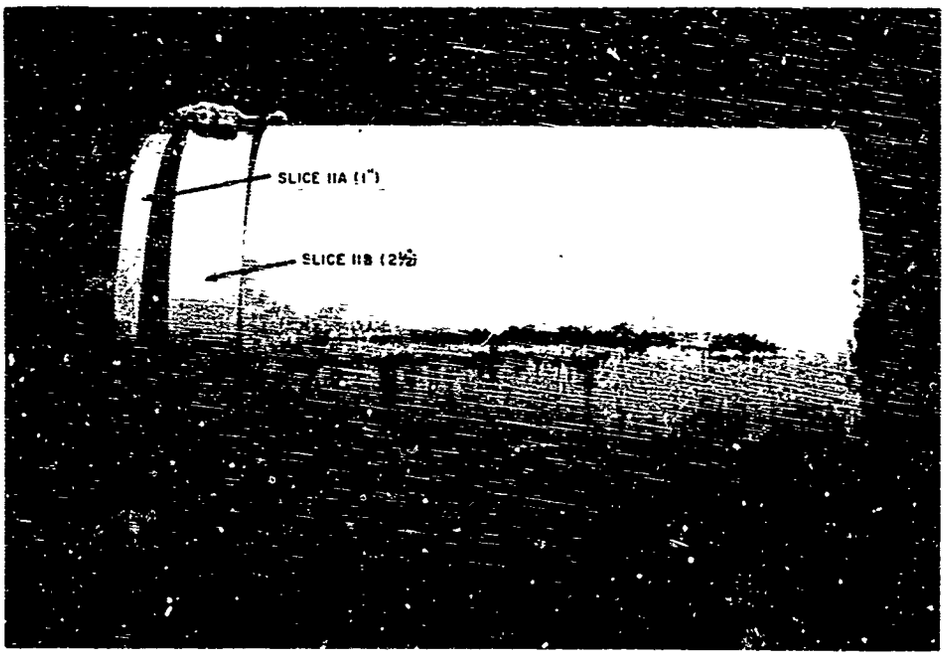

Figure 18. Aluminum 1100-0 Ingot

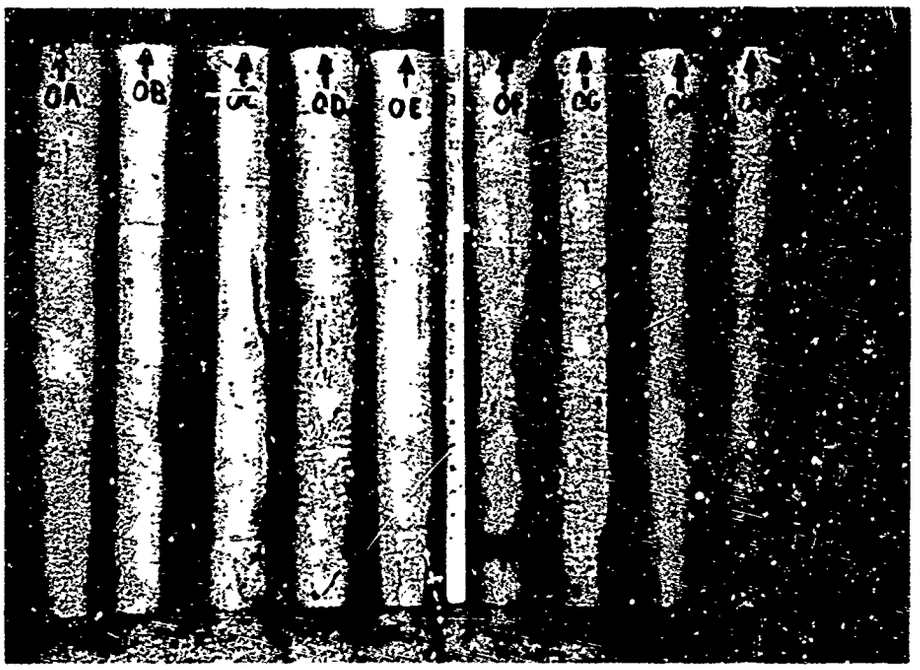

Figure 19. Aluminum 7075-0 Ingots

Figure 20. Aluminum 7075-T6 Ingots

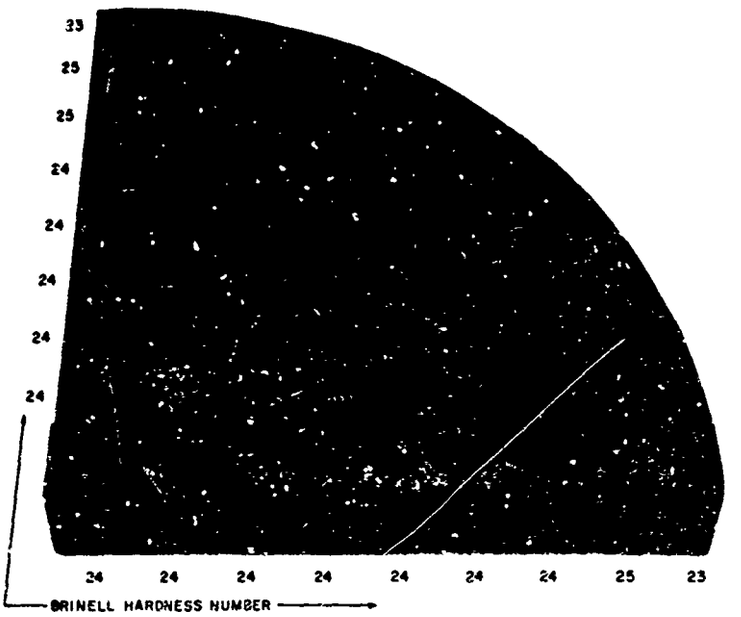

Figure 21. Brinell Hardness Traverse of 1100-0

Aluminum 7075-0

A 1-in. long section was removed from the top of the ingot which was designated "stub". The sawn surface was ground smooth and polished for the Brinell hardness determination with a 500-kg load applied for 30 sec to a 10-mm diameter steel ball. Hardness measurements were made at 0.4-in. intervals and resulted in a range of 57.9 to 59.8 BHN over a 1.2-in. radius as shown in Figure 22.

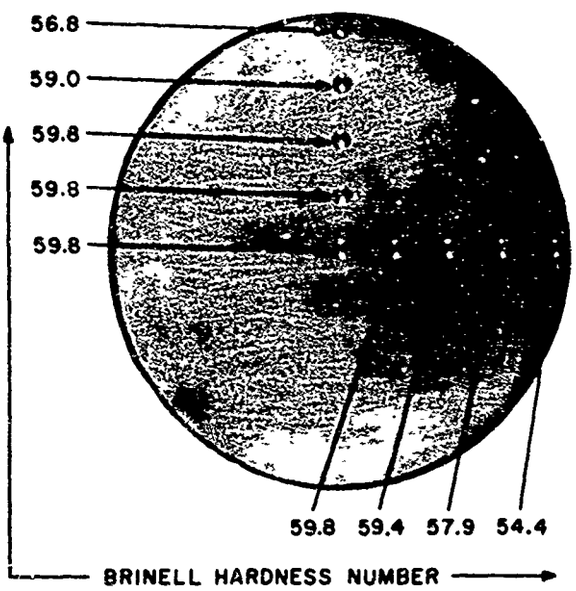

Figure 22. Brinell Hardness Traverse of 7075-0

Aluminum 7075-T6

A 1-in. long section was removed from the top of the ingot designated No. 6A as shown in Figure 20. The sawn surface was ground smooth and polished for Brinell hardness determination with a 500-kg load applied for 30 sec to a 10-mm diameter steel ball. Hardness measurements were made at 0.4-in. intervals and resulted in a range of values from 158 to 162 BHN over a 1.2-in. radius. Verification measurements were made with 1000 to 3000-kg loads. The hardness values obtained with the 1000-kg load were one to two numbers higher than those with the 500-kg load, while the values with the 3000-kg load were six to nine numbers higher; i.e., 158, 159, and 165 BHN, with the 500, 1000, and 3000 kg load respectively.

In addition to the Brinell hardness values summarized in Figure 22, the Knoop hardness values were also determined to indicate the relation between the micro-(Knoop) and macro-(Brinell) hardness tests. As would be expected, the Brinell hardness test is not as sensitive to micro-structure effects as the Knoop test, since the 10-mm ball in the Brinell test measures an average hardness by indenting numerous crystal grains in the specimen and, therefore, levels out the effects of any mechanical anisotropy.

GRAIN SIZE

The grain size was determined for each of the alloy types and found to correspond to the ASTM designation[2] given in Table 4.

TABLE 4

GRAIN SIZE OF THREE ALUMINUM TYPES

Alloy Type	ASTM Grain Size Designation
1100-0	No. 0 to 00
7075-0	No. 5
7075-T6	No. 5

TENSILE TESTING

Tensile specimens were prepared according to the specification shown in Figure 23; a typical tensile bar is shown in Figure 24. Longitudinal and transverse specimens were obtained in duplicate from the 7075 ingots as indicated in Figure 25 and from the 1100-0 ingot as indicated in Figure 26.

DESCRIPTION AND OPERATION OF APPARATUS

Nunes and Larson[3] utilized the basic features of the diameter gage designed by Powell et al.,[4] but added a pair of cantilever arms 90° opposite the originally designed pair. Located on the lower end of the cantilever arms are knife-edge fingers, adjustable to the specimen cross section, that act as sensing elements by deflecting when the specimen deforms. These deflections are converted to electrical signals at the strain gage component, and the cantilever arm is an insulator used to

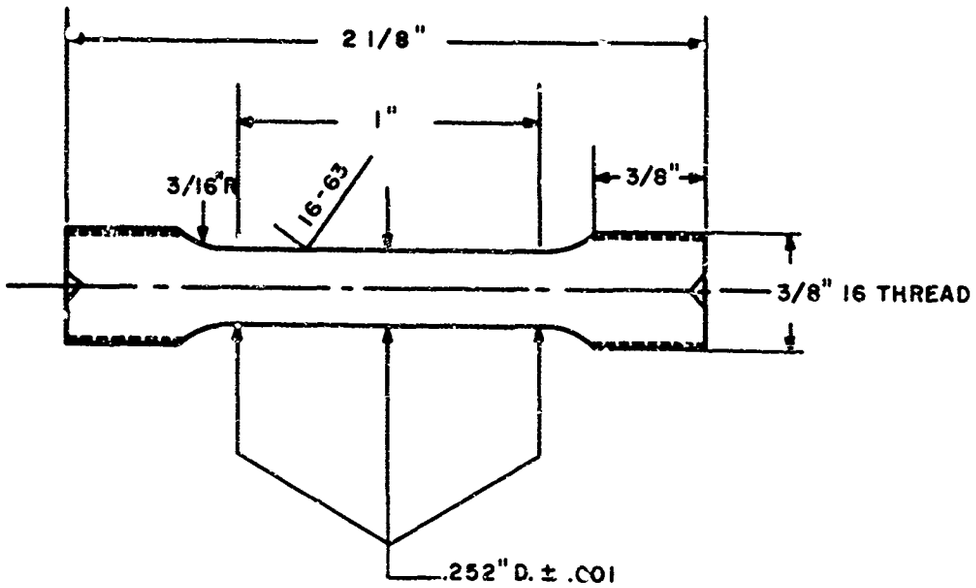

CUT COLD AND SLOW
GRIND CAREFULLY

Figure 23. Specification for Tensile Test Specimen

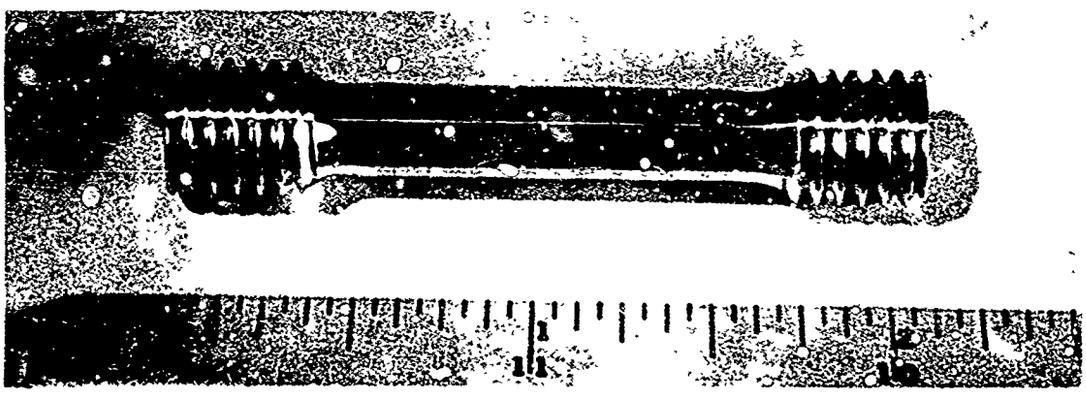

Figure 24. A Typical Tensile Test Specimen Prior to Surface Preparation

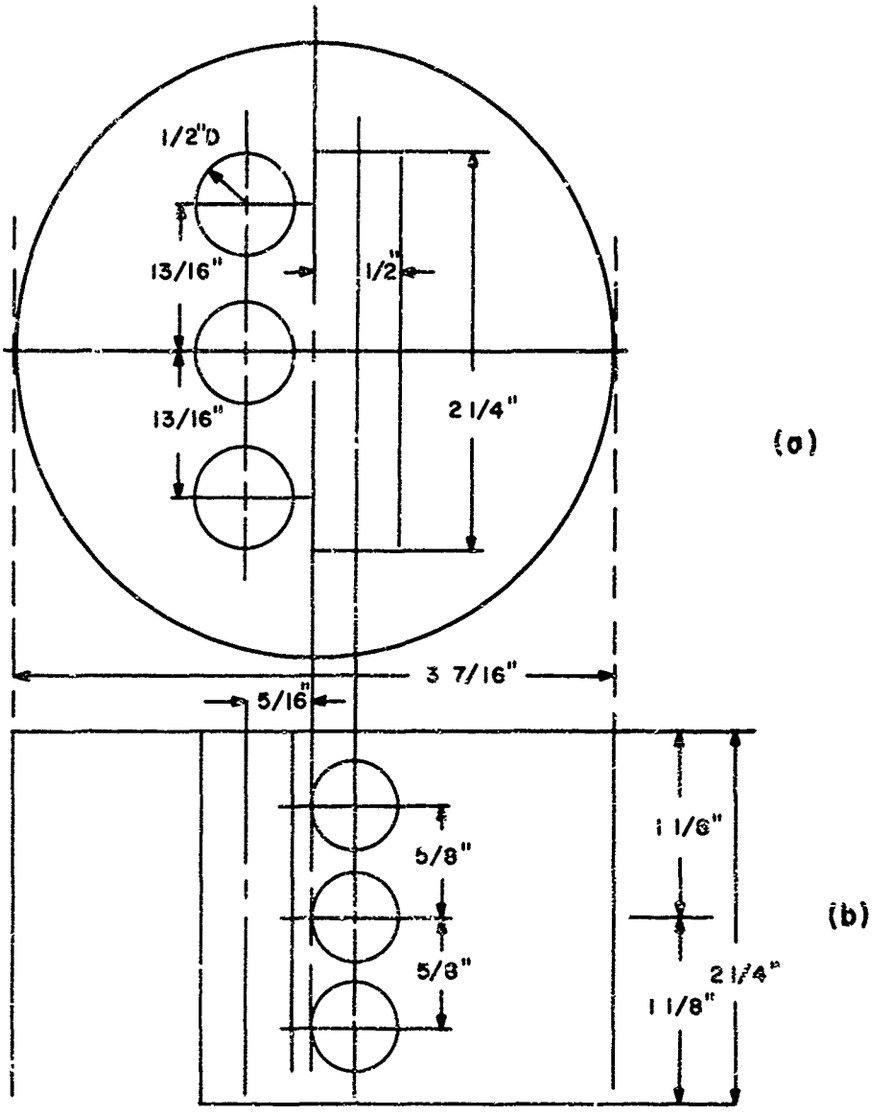

Figure 25. Positions from Which the Tensile Specimens were Selected from the 7075 Ingots ((a) longitudinal, (b) transverse)

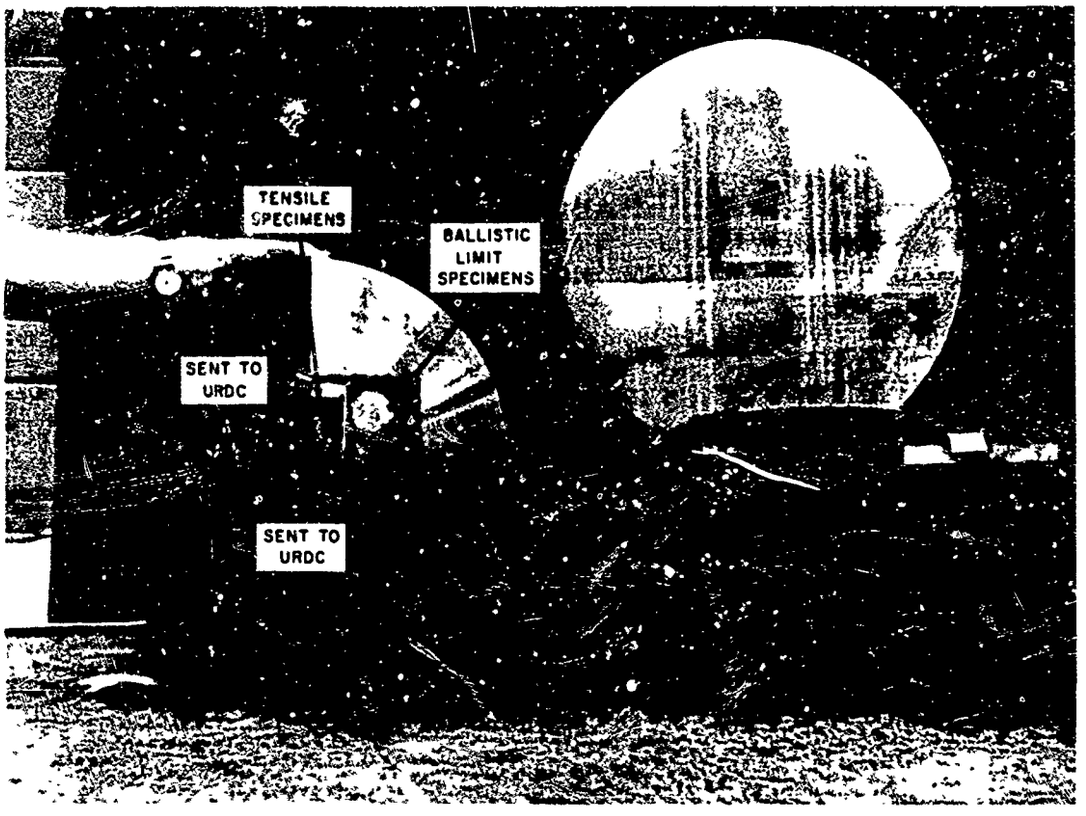

Figure 26. Positions from Which the Tensile Specimens were Selected from the 1100-0 Ingot

minimize the temperature gradient effects obtained at low testing-temperatures. An epoxy resin adhesive was used to bond the strain gages on the sides of the cantilever arm assembly. A spring was attached to each arm to reduce any vibration picked up by the arm as it traversed the specimen surface. The sleeve, to which the cantilever arm assembly is attached, was made to align with the shaft holding the tension specimen and was free to slide vertically along the shaft. By attaching a rack gear and a motor to the assembly, it was possible to obtain continuous travel along the specimen surface at a predetermined rate set by a Variac control. The limit switches were provided to control the total travel of the diameter gage assembly in either direction and are adjustable to the specimen gage length.

Figure 27 is a wiring diagram of the Wheatstone bridge circuit employed in this assembly. The C_1 and C_2 resistors are placed on the compressive side of the cantilever arms, with the T_1 and T_2 resistors placed on the tension side as shown. Since this circuit is the same for both pairs of arms, signals are obtained independently in the width and thickness directions of a specimen.

The diameter gage assembly is relatively compact and is positioned over the specimen in such a manner that a liquid coolant tank can be placed into the setup for low-temperature testing. Two shafts, mounted between the platen heads of the Tinius Olsen testing machine, hold the specimen. One of these is simply a pinned holder,

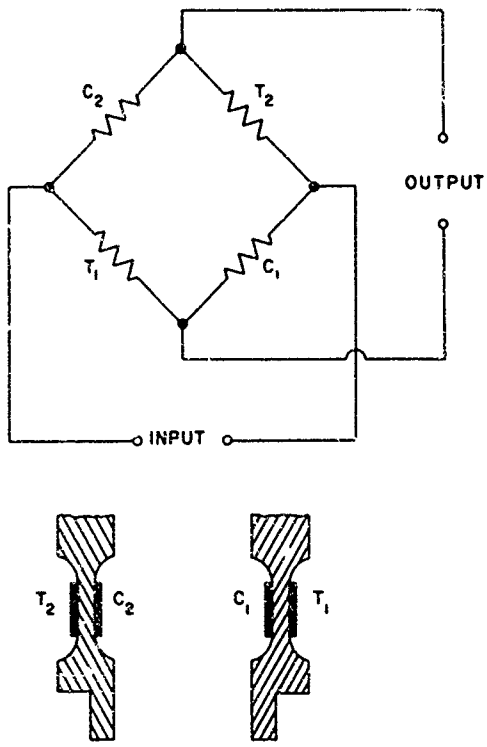

Figure 27. Wheatstone Bridge Circuit and Strain Gage Location on Cantilever Arms (after Nunes and Larson[3])

while the other is made up of two parts — a holder and a dynamometer through which the load was recorded. A Sanborn 150 six-channel oscillographic recorder was used to obtain a record of the load-profile measurements.

All tests were run at a constant cross-head speed to give an initial strain rate of $0.01\ min^{-1}$. Records of load versus cross-head displacement were used to obtain yield strength values at the lower testing temperatures. Tests conducted at room temperature were run with a snap-on extensometer that was attached to the specimen until a 0.2% offset yield was attained and then the diameter gage was retracted into the up position. After the desired yield was obtained, the extensometer was removed and the diameter gage was set into operation to record the resulting deformation to fracture.

Calibration of the recorder and balancing of the Wheatstone bridge circuits were accomplished with the specimen in position for testing but without applying any load. After calibrating and balancing, the load pen was adjusted to the zero load line. Then a minor load was placed on the specimen and the stylus pen of the recorder, which is used to measure the diameter, was positioned to a known reference line. Maintaining a constant and continuous profile record was accomplished by running the recorder chart and the diameter gage at constant predetermined speeds (2.5 mm/sec).

Room temperature tensile specimens were completely immersed in alcohol and the cryogenic tests were made with the specimens immersed in either liquid nitrogen (-196°C) or a carbon dioxide-isopentane (-80°C) mixture. The experimental tensile

data (summarized in Table 5 of the Appendix) can be compared with the published data for these alloys (Table 6 in Appendix).

MECHANICAL PROPERTY DATA

Because of the unusual manner of plotting the actual stress in terms of the logarithm of the extensions, it appeared that the area subtended by the stress curve can have no real meaning. An investigation of the nature of this area has proved differently.

Broadly speaking, the mechanical work performed by a test is the integral of the load F by the increments of the extension

$$W = \int_{L_o}^{L} F \, dL \ .$$

The dimensions of the specimen are eliminated by referring the work expended to the initial volume V_o of the specimen under test. Let the initial cross-sectional area of the specimen be A_o and the test length of the specimen be L_o. Then, we have

$$w = \frac{W}{V_o} = \int_{L_o}^{L} \frac{F}{A_o} \cdot \frac{dL}{L_o} \ .$$

It is customary to express F/A_o as the nominal (or average) stress σ, and

$$\int_{L_o}^{L} \frac{dL}{L_o} = \frac{L - L_o}{L_o} = \frac{L}{L_o} - 1$$

as the nominal (or average linear) strain ϵ. Then the specific work w becomes

$$w = \int_{o}^{\epsilon} \sigma d\epsilon \ .$$

Thus the work expended is represented by the area subtended by the conventional stress plotted as a function of the conventional strain.

In cases such as flow tests where the strain is very great, it is thought that the nominal stress (dependent upon the original cross sectional area) loses much of its physical meaning and is more and more replaced by the actual (true) stress (dependent upon the actual cross section supporting the load). Simultaneously the nominal (average) strain has been replaced by the natural (true) strain. the differential of which is referred to the actual rather than the initial test length of the specimen.

If and when the changes in density and volume of the specimen undergoing the test may be neglected, this new way of expressing the stress strain relation has surprising merit. If we may write

$$V_o = A_o L_o = AL \ ,$$

the specific work w may be written

$$w = \int_{L_o}^{L} \frac{F}{A_o} \cdot \frac{dL}{L_o} = \int_{L_o}^{L} \frac{F}{A} \cdot \frac{dL}{L} \ ,$$

in which F/A is the actual (true) stress σ_a and

$$\int_{L_o}^{L} \frac{dL}{L} = \log_e \frac{L}{L_o}$$

appears as the natural (true) strain ϵ_n. We may thus also write

$$w = \int_{o}^{\epsilon_n} \sigma_a d\epsilon_n$$

and find that the subtended area of the actual (true) stress in terms of the natural (true) strain does indeed represent the specific work expended during the test. Moreover, this representation gives the actual (true) stress existing at any instant in the specimen under test and the natural (true) strain produced by same without any reference to previous history.

In Figure 28, the actual (true) stress is plotted in terms of the natural (true strain for the transverse specimen of 1100-0 at -80°C. The area subtended by the curve in the graph does not seem to represent the work spent and absorbed by the specimen undergoing the test. To determine this amount of work, the data in Table 7 of the Appendix must be recalculated and the graph replotted to give the load applied in terms of the extension of a unit length of the specimen, that is, in terms of the strain. The load can be determined as the nominal (average) stress, which is the stress referred to the original cross-sectional area.

The nominal (average) strain of a specimen that is elongated from length L_o to length L is

$$\epsilon = \int_{L_o}^{L} \frac{dL}{L_o} = \frac{L - L_o}{L_o} = \frac{L}{L_o} - 1 \ .$$

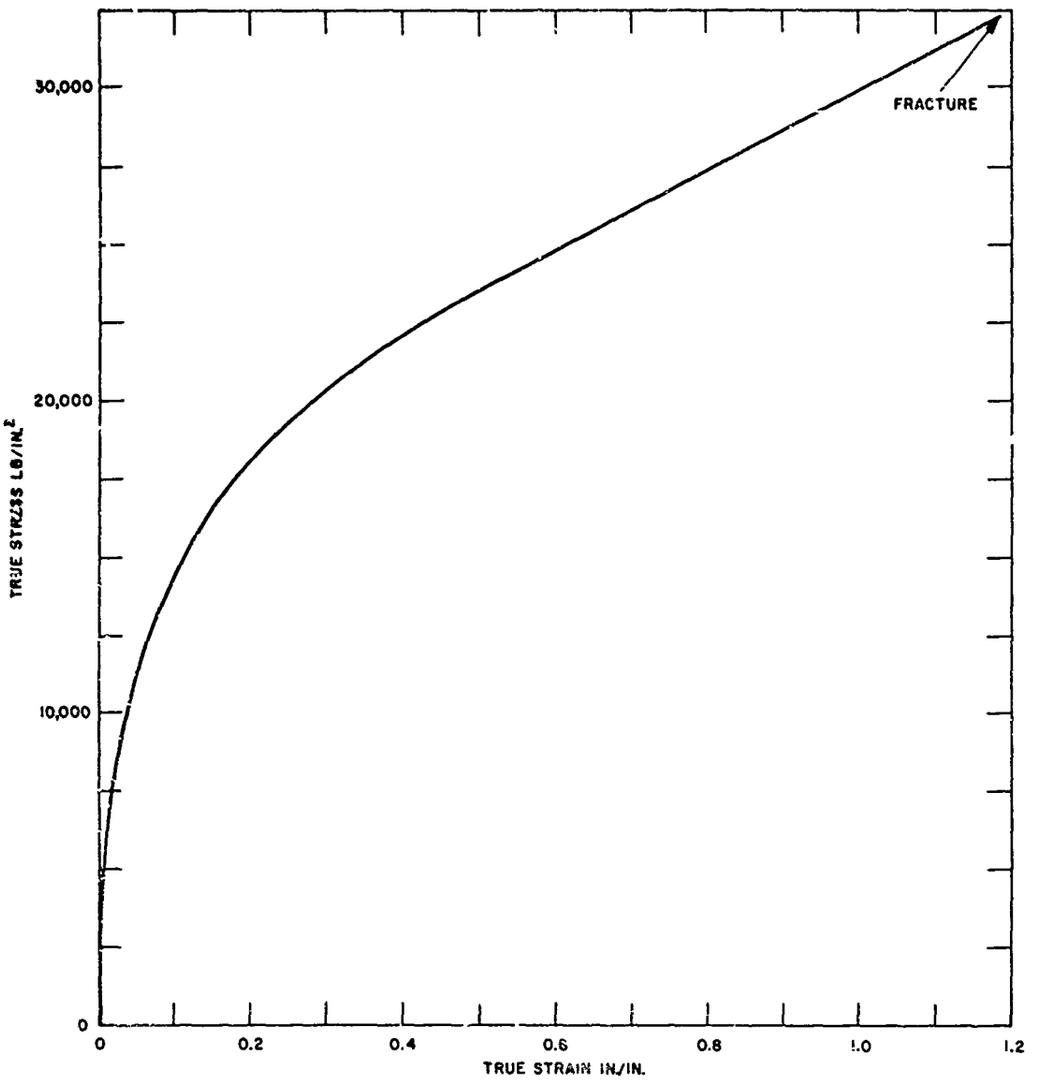

Figure 28. True Stress Versus True Strain for Transverse Specimen of 2100-0 at -80°C

When L_o is taken as unity, the strain is simply

$$\epsilon = L - 1 \ .$$

The natural (true) strain used currently in problems of flow reflects the fact that after having flowed the material does not "remember" what its initial length was, so in subsequent flows it sheds little light on the phenomenon to relate the new increase in length to the original length. Therefore it has appeared much more appropriate to

relate it to the current length of the specimen. Thus the "natural" strain is given as

$$\epsilon_n = \int_{L_o}^{L} \frac{dL}{L} = \log_e \frac{L}{L_o} \quad .$$

When the initial length of the specimen is taken as unity, the natural strain is simply

$$\epsilon_n = \log_e L \quad .$$

Under such circumstances the relation between natural (true) and nominal (average) strain is simply

$$\epsilon = e^{\epsilon_n} - 1 \quad .$$

Pertinent data are summarized in Table 8 of the Appendix.

To obtain the nominal (average) stress, the original cross section must be determined. Since the nominal stress is not given, it can be determined from the cross sections during the test and the simultaneous lengths L can be calculated. If one neglects the change in volume of the specimen during the test, the product of the initial cross-section and specimen length must be equal to the product of the current cross section and the current specimen length:

$$A_o \cdot L_o = A \cdot L = \text{Volume} \quad .$$

To test the rigorousness of this simplification, the fifth column in Table 8 has been added; this gives the volume of a part of the specimen initially 1 in. long. The mean comes out as 0.0498667 cu in. with a maximum variation of + 0.217 and -0.238%, which is remarkably accurate considering the areas were given to three significant figures only. Dividing the load by the original cross section of 0.0498667, one obtains the nominal stresses during the test (first column of Table 8)

The work per cubic inch of material is given then as

$$w = \int_{o}^{\epsilon} \sigma d\epsilon$$

and is represented by the area subtended by the curve. At the scale used, every square centimeter of the graph represents 40 in.-lb/cu in. and every square millimeter represents 4/10 in.-lb. The area under the curves was measured with a planimeter. The areas under the two separate curves for the same test differ from one another by count by 1/2%; Figure 28 gives 27,205 in.-lb/cu in. of specimen,* and the nominal stress

*Planimeter measurement was 27.584 in.-lb/cu in. of specimen.

versus nominal strain curve gives 27,340 in.-lb/cu in. The lack of points between the two largest strains must be blamed for this discrepancy.

It is apparent that almost half the work was expended in the last straining step, from $\epsilon = 1.05033$ to $\epsilon = 2.19313$, for which the plotting of the curve is somewhat uncertain because of the lack of experimental points. All the expended energy, less a negligible amount stored as elastic strain energy in the specimen under test, is used as flow strain energy.

REFERENCES

1. R. F. Rolsten and H. H. Hunt, AIAA Journal 1, 1893-1895 (1963).

2. American Society for Testing and Materials," Methods for Determining the Average Grain Size of Metals," ASTM Designation: E112 (no date).

3. J. Nunes and F. R. Larson, "A Method for Determining the Plastic Flow Properties of Sheet and Round Tension Test Specimens," Proceedings of the American Society for Testing Materials 61, 1349-1361 (1961).

4. G. W. Powell, E. R. Marshall, and W. A. Backofen, "A Diameter Gage and Dynamometer for True Stress-Strain Tension Tests at Constant True Strain Rate," Proceedings of the American Society for Testing Materials 55, 797-809 (1955).

APPENDIX

SUMMARY OF METALLURGICAL DATA

TABLE 5

EXPERIMENTAL TENSILE DATA

Alloy	Test Temp. (°C)	Strength (psi)	
		Yield	Ultimate
1100-0	24	4.2	12.1
1100-0	24	3.8	12.6
1100-0	-80	4.2	15.1
1100-0	-80	4.0	14.9
1100-0	-196	6.4	25.7
1100-0	-196	6.7	25.7
7075-0	24	13.2	34.0
7075-0	24	13.0	33.2
7075-0	-80	13.8	35.8
7075-0	-80	13.6	34.7
7075-0	-196	16.2	18.0
7075-0	-196	16.6	48.2
7075-T6	24	68.9	79.4
7075-T6	24	70.5	80.5
7075-T6	-80	73.2	85.1
7075-T6	-196	81.4	91.8
7075-T6	-196	80.2	91.2

TABLE 6

PUBLISHED METALLURGICAL DATA
(Alcoa Aluminum Handbook)

Alloy	Test Temp. (°C)	Strength (psi)		Brinell Hardness Number 500-kg load, 10 mm ball	Specific Gravity	Chemical Composition Limits (%)							
		Yield	Ultimate			Si	Fe	Cu	Mn	Mg	Cr	Zn	Ti
1100-0	24	5,000	13,000	23	2.71	1.0	1.0	0.20	0.05	–	–	0.0	–
1100-0	-190	6,000	24,000	–									
7075-0	24	15,000	33,000	60	2.80	0.50	0.7	1.2-2.0	0.30	2.1-2.9	0.18-0.40	5.1-6.1	–
7075-0	-190			–									
7075-T6	24	73,000	83,000	150	2.80	0.50	0.7	1.2-2.0	0.30	2.1-2.9	0.18-0.40	5.1-6.1	0.20
7075-T6	-190	92,000	102,000	–									

TABLE 7

TRANSVERSE SPECIMEN OF 1100-0 AT -80°C

Diameter (in.)		Load (psi)	Area (in^2)	True Strain (in./in.)	True Stress (ksi)
D_1	D_2				
0.252	0.252	–	–	–	–
0.251	0.251	340	0.04948	0.0080	6.871
0.250	0.250	390	0.04909	0.0159	7.945
0.249	0.249	420	0.04870	0.0238	8.624
0.248	0.248	470	0.04831	0.0317	9.729
0.247	0.247	500	0.04792	0.0396	10.434
0.246	0.2464	535	0.04753	0.0467	11.256
0.244	0.245	580	0.04695	0.0611	12.353
0.242	0.243	620	0.04619	0.0765	13.423
0.240	0.2416	650	0.04554	0.0909	14.273
0.238	0.2396	675	0.04478	0.1071	15.074
0.236	0.2376	695	0.04404	0.1241	15.781
0.234	0.2356	715	0.04330	0.1409	16.513
0.232	0.234	720	0.04264	0.1567	16.885
0.228	0.232	735	0.04155	0.1833	17.690
0.224	0.228	745	0.04012	0.2177	18.569
0.220	0.224	750	0.03871	0.2533	19.375
0.218	0.222	735	0.03801	0.2708	19.863
0.216	0.220	755	0.03733	0.2899	20.226
0.214	0.218	755	0.03664	0.3089	20.606
0.212	0.216	755	0.03597	0.3268	20.990
0.207	0.212	745	0.03447	0.3696	21.613
0.202	0.208	735	0.03301	0.4124	22.266
0.192	0.198	710	0.02986	0.5124	23.778
0.182	0.190	680	0.02717	0.6076	25.028
0.172	0.180	640	0.02433	0.7181	26.305
0.135	0.1472	500	0.01563	1.161	31.990

TABLE 8

NOMINAL STRESS-STRAIN DATA WITH VOLUME OF SPECIMEN

Nominal Stress σ	Natural or True Strain $\epsilon_n = x$	Specimen Length $L = e^x$	Average Strain $\epsilon = e^x - 1$	Specimen Volume $V = A \cdot L$
6,818	0.008	1.00804	0.00804	0.049797
7,821	0.016	1.01614	0.01614	0.049892
8,422	0.024	1.02430	0.02430	0.049883
9,425	0.032	1.03253	0.03253	0.049871
10,027	0.040	1.04082	0.04082	0.049855
10,727	0.047	1.04813	0.04813	0.049891
11,631	0.060	1.06184	0.06184	0.049906
12,433	0.077	1.08004	0.08004	0.049898
13,035	0.091	1.09528	0.09528	0.049835
13,536	0.108	1.11406	0.11406	0.049910
13,937	0.126	1.13439	0.13439	0.049913
14,338	0.142	1.15259	0.15259	0.049907
14,438	0.158	1.17118	0.17118	0.049892
14,739	0.183	1.20082	0.20082	0.049884
14,940	0.218	1.24360	0.24360	0.049868
15,040	0.254	1.28918	0.28918	0.049941
15,140	0.272	1.31259	0.31259	0.049928
15,140	0.290	1.33644	0.33644	0.049849
15,140	0.308	1.36071	0.36071	0.049802
15,140	0.327	1.38681	0.38681	0.049975
14,940	0.365	1.44052	0.44052	0.049748
14,739	0.413	1.51134	0.51134	0.049874
14,238	0.513	1.67030	0.67030	0.049775
13,636	0.603	1.82760	0.82760	0.049760
12,834	0.718	2.05033	1.05033	0.049823
10,027	1.161	3.19313	2.19313	—

Unclassified
Security Classification

DOCUMENT CONTROL DATA - R&D

(Security classification of title, body of abstract and indexing annotation must be entered when the overall report is classified)

1. ORIGINATING ACTIVITY *(Corporate author)*

Technical Operations Research
Burlington, Massachusetts

2a. REPORT SECURITY CLASSIFICATION
Unclassified

2b. GROUP

3. REPORT TITLE

HYPERVELOCITY IMPACT STUDIES

4. DESCRIPTIVE NOTES *(Type of report and inclusive dates)*

Final Report 1 February to 15 October 1965

5. AUTHOR(S) *(Last name, first name, initial)*

Roisten, Robert F.

6. REPORT DATE	7a. TOTAL NO. OF PAGES	7b. NO. OF REFS
October 1965	53	11

8a. CONTRACT OR GRANT NO. AF 33(615)-01333	9a. ORIGINATOR'S REPORT NUMBER(S) AFML-TR-66-40
b. PROJECT NO. 7360	
c. TASK 736006	9b. OTHER REPORT NO(S) *(Any other numbers that may be assigned this report)* TO-B 65-103
d.	

10. AVAILABILITY/LIMITATION NOTICES
Foreign announcement and dissemination of this report by DDC is not authorized.

11. SUPPLEMENTARY NOTES	12. SPONSORING MILITARY ACTIVITY
	Air Force Materials Laboratory, RTD Air Force Systems Command Wright-Patterson Air Force Base, Ohio

13. ABSTRACT

Two different problems related to hypervelocity impact were studied. The first involved the formation of a rippled surface produced at the interface of a stack of plates impacted by a projectile. The rippled structure was produced, as observed in cross section, as a sine wave, a sawtooth structure, and as oriented waves with a peaked crest. Some plates were welded permanently; others separated as a result of failure in the base metal. A plausible explanation for the ring structure was found. The second problem involved the preparation and evaluation of homogeneous 1100-0, 7075-0, and 7075-T6 aluminum ingots for use as hypervelocity impact targets. An attempt was made to control grain size and to provide equiaxed grains. Tensile test data obtained in longitudinal and transverse specimens include yield and ultimate and true stress to fracture.

DD FORM 1 JAN 64 1473

Unclassified
Security Classification

14. KEY WORDS	LINK A		LINK B		LINK C	
	ROLE	WT	ROLE	WT	ROLE	WT
Hypervelocity particle impact Metallurgy Tensile testing Materials response Impact welding						

INSTRUCTIONS

1. ORIGINATING ACTIVITY: Enter the name and address of the contractor, subcontractor, grantee, Department of Defense activity or other organization *(corporate author)* issuing the report.

2a. REPORT SECURITY CLASSIFICATION: Enter the overall security classification of the report. Indicate whether "Restricted Data" is included. Marking is to be in accordance with appropriate security regulations.

2b. GROUP: Automatic downgrading is specified in DoD Directive 5200.10 and Armed Forces Industrial Manual. Enter the group number. Also, when applicable, show that optional markings have been used for Group 3 and Group 4 as authorized.

3. REPORT TITLE: Enter the complete report title in all capital letters. Titles in all cases should be unclassified. If a meaningful title cannot be selected without classification, show title classification in all capitals in parenthesis immediately following the title.

4. DESCRIPTIVE NOTES: If appropriate, enter the type of report, e.g., interim, progress, summary, annual, or final. Give the inclusive dates when a specific reporting period is covered.

5. AUTHOR(S): Enter the name(s) of author(s) as shown on or in the report. Enter last name, first name, middle initial. If military, show rank and branch of service. The name of the principal author is an absolute minimum requirement.

6. REPORT DATE: Enter the date of the report as day, month, year, or month, year. If more than one date appears on the report, use date of publication.

7a. TOTAL NUMBER OF PAGES: The total page count should follow normal pagination procedures, i.e., enter the number of pages containing information.

7b. NUMBER OF REFERENCES: Enter the total number of references cited in the report.

8a. CONTRACT OR GRANT NUMBER: If appropriate, enter the applicable number of the contract or grant under which the report was written.

8b, 8c, & 8d. PROJECT NUMBER: Enter the appropriate military department identification, such as project number, subproject number, system numbers, task number, etc.

9a. ORIGINATOR'S REPORT NUMBER(S): Enter the official report number by which the document will be identified and controlled by the originating activity. This number must be unique to this report.

9b. OTHER REPORT NUMBER(S): If the report has been assigned any other report numbers *(either by the originator or by the sponsor)*, also enter this number(s).

10. AVAILABILITY/LIMITATION NOTICES: Enter any limitations on further dissemination of the report, other than those imposed by security classification, using standard statements such as:

(1) "Qualified requesters may obtain copies of this report from DDC."

(2) "Foreign announcement and dissemination of this report by DDC is not authorized."

(3) "U. S. Government agencies may obtain copies of this report directly from DDC. Other qualified DDC users shall request through

_____."

(4) "U. S. military agencies may obtain copies of this report directly from DDC. Other qualified users shall request through

_____."

(5) "All distribution of this report is controlled. Qualified DDC users shall request through

_____."

If the report has been furnished to the Office of Technical Services, Department of Commerce, for sale to the public, indicate this fact and enter the price, if known.

11. SUPPLEMENTARY NOTES: Use for additional explanatory notes.

12. SPONSORING MILITARY ACTIVITY: Enter the name of the departmental project office or laboratory sponsoring *(paying for)* the research and development. Include address.

13. ABSTRACT: Enter an abstract giving a brief and factual summary of the document indicative of the report, even though it may also appear elsewhere in the body of the technical report. If additional space is required, a continuation sheet shall be attached.

It is highly desirable that the abstract of classified reports be unclassified. Each paragraph of the abstract shall end with an indication of the military security classification of the information in the paragraph, represented as *(TS), (S), (C), or (U).*

There is no limitation on the length of the abstract. However, the suggested length is from 150 to 225 words.

14. KEY WORDS: Key words are technically meaningful terms or short phrases that characterize a report and may be used as index entries for cataloging the report. Key words must be selected so that no security classification is required. Identifiers, such as equipment model designation, trade name, military project code name, geographic location, may be used as key words but will be followed by an indication of technical context. The assignment of links, rules, and weights is optional.